A Novel Interaction Between Aging and ER Overload in a Protein Conformational Dementia

Angela Schipanski,*,[1,2] Sascha Lange,*,[1] Alexandra Segref,[†] Aljona Gutschmidt,[†] David A. Lomas,[‡] Elena Miranda,[‡,3] Michaela Schweizer,[§] Thorsten Hoppe,[†,5] and Markus Glatzel*,[5]

* Institute of Neuropathology and [§]Center for Molecular Neurobiology, University Medical Center Hamburg-Eppendorf, 20246 Hamburg, Germany, [†]Institute for Genetics and Cologne Excellence Cluster on Cellular Stress Responses in Aging-Associated Diseases (CECAD), University of Cologne, 50674 Cologne, Germany, and [‡]Department of Medicine, University of Cambridge, Cambridge Institute for Medical Research, Wellcome Trust/Medical Research Council Building, Cambridge CB2 0XY, United Kingdom

ABSTRACT Intraneuronal deposition of aggregated proteins in tauopathies, Parkinson disease, or familial encephalopathy with neuroserpin inclusion bodies (FENIB) leads to impaired protein homeostasis (proteostasis). FENIB represents a conformational dementia, caused by intraneuronal polymerization of mutant variants of the serine protease inhibitor neuroserpin. In contrast to the aggregation process, the kinetic relationship between neuronal proteostasis and aggregation are poorly understood. To address aggregate formation dynamics, we studied FENIB in *Caenorhabditis elegans* and mice. Point mutations causing FENIB also result in aggregation of the neuroserpin homolog SRP-2 most likely within the ER lumen in worms, recapitulating morphological and biochemical features of the human disease. Intriguingly, we identified conserved protein quality control pathways to modulate protein aggregation both in worms and mice. Specifically, downregulation of the unfolded protein response (UPR) pathways in the worm favors mutant SRP-2 accumulation, while mice overexpressing a polymerizing mutant of neuroserpin undergo transient induction of the UPR in young but not in aged mice. Thus, we find that perturbations of proteostasis through impairment of the heat shock response or altered UPR signaling enhance neuroserpin accumulation *in vivo*. Moreover, accumulation of neuroserpin polymers in mice is associated with an age-related induction of the UPR suggesting a novel interaction between aging and ER overload. These data suggest that targets aimed at increasing UPR capacity in neurons are valuable tools for therapeutic intervention.

CONFORMATIONAL disorders are mainly caused by deposition of proteins with conformational changes reducing the function and increasing formation of protein aggregates (Lomas and Carrell 2002; Kikis *et al.* 2010). Despite the fact that protein aggregation occurs in different tissues, neurons are especially sensitive for accumulation of proteins, which could lead to neurodegeneration. While tauopathies, Parkinson disease, and familial encephalopathy with neuroserpin inclusion bodies (FENIB) are commonly characterized by deposition of aggregated proteins in neurons, FENIB specifically exhibits conspicuous protein aggregates in the endoplasmatic reticulum (ER) (Lomas and Carrell 2002).

Serpinopathies, including α_1-antitrypsin deficiency and FENIB, are based on intracellular polymer formation between mutant variants carrying destabilizing point mutations (Lomas and Carrell 2002). Neuroserpin, an axonally secreted protein acts neuroprotectively and plays a role in synaptic plasticity (Borges *et al.* 2010; Wu *et al.* 2010). Serpinopathies are caused by intracellular polymer formation between mutant variants carrying destabilizing mutations that enable insertion of the reactive center loop of one serpin molecule into the β-sheet of another (Lomas and Carrell 2002). For example, FENIB is characterized by intraneuronal accumulation of neuroserpin polymers (Davis *et al.* 2002). To date, six autosomal dominantly inherited mutations have been described (Hagen *et al.* 2011), with the S49P mutation

doi: 10.1534/genetics.112.149088
Manuscript received November 22, 2012; accepted for publication December 26, 2012
Supporting information is available online at http://www.genetics.org/lookup/suppl/doi:10.1534/genetics.112.149088/-/DC1.
[1]These authors contributed equally to this work.
[2]Present address: Swiss Federal Laboratories for Materials Science and Technology Laboratory for Materials– Biology Interaction, 9000 St. Gallen, Switzerland.
[3]Present address: Department of Internal Medicine III and Clinics, University Medical Center Hamburg-Eppendorf, 20246 Hamburg, Germany.
[4]Present address: Department of Biology and Biotechnologies "Charles Darwin" and Pasteur Institute-Cenci Bolognetti Foundation, University of Rome "La Sapienza," p.le Aldo Moro 5, Rome 00185, Italy.
[5]Corresponding authors: E-mail: thorsten.hoppe@uni-koeln.de; and E-mail: m.glatzel@uke.de

causing older age of onset and milder clinical course as compared to the H338R mutation.

Proteostasis, which is disturbed in dementias, encompasses the interplay of translational regulation with protein folding, trafficking, and processing but also assembly or disassembly and degradation of proteins (Kikis *et al.* 2010). Protein degradation, which is essential for proteostasis, is executed by the ubiquitin/proteasome system (UPS) and the autophagy–lysosome pathway (Rubinsztein 2006). Secretory proteins that accumulate in the ER are retrotranslocated into the cytosol and degraded via ER-associated protein degradation (ERAD) (Rubinsztein 2006), which can be upregulated by the UPR (Ron and Walter 2007). The UPR is a signaling program executed by ER transmembrane receptors activating transcription factor 6 (ATF6), inositol requiring kinase 1 (IRE1), and double-stranded RNA-activated protein kinase (PKR)-like endoplasmic reticulum kinase (PERK), aimed at restoring ER homeostasis (Chakrabarti *et al.* 2011). ERAD is essential for degradation of monomeric mutant neuroserpin (Kroeger *et al.* 2009). In cultured cells, accumulation of polymeric neuroserpin leads to activation of NF-κB by the ER overload pathway in the absence of the UPR (Davies *et al.* 2009; Kroeger *et al.* 2009).

Caenorhabditis elegans models expressing aggregation-prone proteins such as polyQ-GFP or fragments of metastable human proteins have helped in deciphering molecular details of protein aggregation and proteostasis (Nollen *et al.* 2004; Garcia *et al.* 2007; van Ham *et al.* 2010). To study mechanisms of protein aggregation in FENIB, we created a disease model in *C. elegans* by introducing FENIB-associated mutations in the neuroserpin homolog SRP-2. Our data suggest that activation of either heat shock response or UPR influences aggregation of mutant SRP-2 in worms, while in FENIB mice, transient activation of the UPR diminishes with age and correlates with an increase in polymeric neuroserpin. These data support a crucial role for neuronal proteostasis mechanisms in conformational dementias.

Materials and Methods

Mouse experiments

Experiments were carried out in accordance with institutional guidelines of the University Medical Centre Hamburg-Eppendorf. Mice overexpressing mutant (*Tg*NS^{S49P}) and wild-type [*Tg*(NS)] human neuroserpin (Galliciotti *et al.* 2007) were used. Unless stated otherwise, three mice per genotype were used at 8, 12, 20, 34, 45, 64, and >80 weeks of age.

Nematode strains and maintenance

Standard conditions were used for *C. elegans* propagation and crosses at 20° (Brenner 1974). Mutations and transgenes used in this study are listed as follows: *hsf-1(sy441)I*, *ire-1(v33)II*, *unc-119(ed3)III*, *atf-6(ok551)X*, and *pek-1(ok275)X*. Bristol N2 was used as a wild-type strain. *nhx-2*::*mCherry*::*lgg-1*; *myo-2*::*GFP* was provided by Cliff J. Luke.

Generation of transgenic nematodes

For *srp-2*::*srp-2*::*YFP*, the 7.1-kb fragment containing the promoter, full-length *srp-2*, and 3′-UTR was cloned into the YFP expression vector pLN022yfp. For *unc-54*::*srp-2*::*YFP*, a truncated *unc-54* promoter of pPD88.27 and full-length *unc-54* 3′-UTR were fused to full-length (1.6-kb) *srp-2* and then cloned into pLN022yfp. *srp-2*::*srp-2*^{H302R}::*YFP* and *unc-54*::*srp-2*^{H302R}::*YFP* were created by site-directed mutagenesis using the Quikchange Lightning kit according to the manufacturer's instruction (Agilent technologies). Transgenic worms were generated by microparticle bombardment of 7 μg DNA using the Biolistic PDS-1000/HE (Bio-Rad) gene gun (Praitis *et al.* 2001).

RNAi

RNA interference was performed at 20° using the feeding method (Kamath *et al.* 2001). Synchronized L1 larvae were placed on IPTG-containing NGM plates (1 mM) seeded with *Escherichia coli* [HT115(DE3)] expressing double-stranded RNA as described (Timmons and Fire 1998).

Imaging and fluorescence recovery after photobleaching analysis

For *C. elegans* immunostaining, synchronized young adults were fixed, permeabilized, and stained with rhodamine-phalloidin (Molecular Probes) or DAPI (Sigma-Aldrich) as described (McIntire *et al.* 1992; Nonet *et al.* 1993). Worms were imaged using an Axioimager (Zeiss) or an Ultraview Vox spinning disc confocal (Perkin Elmer) microscope and analyzed with either Axiovision 4.7 (Zeiss) or Volocity 5 (Perkin Elmer) software. Fluorescence recovery after photobleaching (FRAP) analysis was performed as previously described (Brignull *et al.* 2006).

For immunohistochemistry of mice, brains were processed into 3-μm thin paraffin sections and stained using antibodies against NeuN (Chemicon), activated caspase-3 (R&D Bisosystems), and neuroserpin (Santa Cruz). Immunosignals for above-mentioned antibodies were quantified in the entire CA1 and CA2 hippocampal region (Galliciotti *et al.* 2007) at three anatomically matched levels with an Axioscope bright field microscope and Axiovision 4.1 (Zeiss) software (Sepulveda-Falla *et al.* 2011).

Electron microscopy

For preembedding Diaminobenzidin (DAB) analysis, 150-μm-thick sagittal vibratome sections were incubated with anti-neuroserpin antibody (1:2000) (Miranda *et al.* 2004). Sections were further processed according to Lappe-Siefke *et al.* (2009). For postembedding immunogold labeling, small pieces of cryoprotected cortices were mounted on specimen holders and immersed in liquid nitrogen. Ultrathin sections (80 nm) were cut and labeled according to Slot and Geuze (2007). Imaging was done with a Zeiss EM 902.

C. elegans motility assay

To measure motility, staged young adult nematodes were placed individually in a drop of M9 buffer, following 1-min

acclimatization; completed body bends were counted for 1 min with at least 15 animals per experiment.

C. elegans generation time

Fifteen adult hermaphrodites were allowed to lay eggs for 4 hr at 20° to obtain a population of synchronized embryos. After removal of the adult worm, progenies were monitored for their developmental stage after 65 or 70 hr, respectively. At least three independent experiments were conducted.

Autophagy

Synchronized L1 worms were exposed for 48 hr to RNAi specific for genes required for autophagy, *bec-1*, *unc-51*, *lgg-1*, or to the empty RNAi feeding vector pPD129.36 (control). Subsequently the amount of aggregates in the head region of 10 worms was counted. As a control for efficient inhibition of the autophagy pathway, autophagosome formation of *nhx-2*::*mCherry*::*lgg-1*; *myo-2*::*GFP* worms was visualized upon RNAi treatment following 4 hr starvation as previously described (Miedel *et al.* 2012).

SDS–PAGE and immunoblotting

Tissue from mice or worms was lysed with either SDS sample buffer, SDS containing and SDS-free RIPA, or worm lysis buffer (Gidalevitz *et al.* 2009). Western blotting was performed under denaturing and nondenaturing (Miranda *et al.* 2004) conditions using antibodies against GFP (Clonetch), α-tubulin (Sigma-Aldrich), ATF6 (Imgenex), eIF2α/eIF2αP (Cell Signaling), neuroserpin (Miranda *et al.* 2008), LC3-I/-II (Thelen *et al.* 2012), and actin (Sigma-Aldrich). Visualization and quantification was done with either Imager Gel Doc System and Quantity One software (Bio-Rad) or Typhoon Trio scanner with ImageQuant software (GE Healthcare). Changes in protein expression of ATF6, LC3-I, LC3-II, or eIF2αP were calculated by normalization to β-actin or eI2Fα in three independent experiments, where wild-type values were set to one (Glatzel *et al.* 2001; Thelen *et al.* 2012).

Analysis of XBP1 mRNA splicing

RNA extraction and cDNA synthesis was performed with RNA Miniprep (Stratagene) and RevertAid (Fermentas) kits. PCR and restriction digestion with *Pst*I, discriminating spliced and unspliced forms of XBP1, was performed as described before (Calfon *et al.* 2002).

ELISA

The ELISA was performed according to published protocols (Miranda *et al.* 2008). Three mice per genotype and timepoint were analyzed.

Data analysis

For all experiments, mean ±SEM is indicated. Statistical comparison among groups was calculated using two-tailed Student's *t*-test with a significance value of $*P \leq 0.05$ or $**P \leq 0.01$.

Results

Accumulation of polymeric neuroserpin in the ER correlates with neurodegeneration

To study the relation between deposition of polymeric neuroserpin and neurodegeneration, we performed time course experiments with mice expressing the S49P mutant of neuroserpin, *Tg*(NS^{S49P}) or wild-type neuroserpin *Tg*(NS). Previous studies suggested that mutant neuroserpin accumulates intraneuronally in perinuclear compartments compatible with ER localization (Davis *et al.* 1999; Galliciotti *et al.* 2007). Using conventional and immunoelectron microscopy, we demonstrate progressive accumulation of mutant neuroserpin (Figure 1, A and B) and ER localization of inclusion bodies immunolabeled for neuroserpin in *Tg*(NS^{S49P}) mice (Figure 1C). Using nondenaturing gels, the polymeric nature of these aggregates became apparent (Figure 1D). Interestingly, the amount of neuroserpin deposits gradually raised, reaching a first plateau between weeks 34 and 45, followed by a sharp increase to week 64 and a second peak around week 80 (Figure 1B). Since it has been suggested that accumulation of polymeric proteins correlates with neurodegeneration (Davis *et al.* 2002; Lomas and Carrell 2002), we assessed neuronal loss and apoptotic cell death morphologically. *Tg*(NS^{S49P}) but not *Tg*(NS) mice display neuronal loss as quantified by immunostaining for the neuronal marker NeuN, labeling neuronal nuclei, in the CA1 and CA2 region of the hippocampus at 45 and 80 weeks of age (Figure 1, E and F). This was accompanied by a mild induction of apoptosis as assayed by positive staining for activated caspase-3 (Figure 1, G and H). Thus, we demonstrate that FENIB mice show considerable neurodegeneration and mild induction of apoptotic cell death. Although the correlation between increase in aggregated neuroserpin within the ER and apoptosis is not strict, it may contribute to neurodegeneration in FENIB mice.

Analysis of SRP-2 aggregation in C. elegans

To further address molecular mechanisms underlying aggregation in serpinopathies, we generated a *C. elegans* model for serpin aggregation. Worms do not encode a direct homolog of neuroserpin, but express nine serpin-like proteins, which show highly conserved structural characteristics (Pak *et al.* 2004; Luke *et al.* 2006). Carrying out *in silico* analysis, we identified SRP-2 as the closest homolog to mammalian neuroserpin based on protein sequence similarity and conservation of critical domains (Pak *et al.* 2004) (Figure 2A and Supporting Information, Figure S1). This bioinformatic approach identified codon 302 of *C. elegans srp-2* corresponding to codon 338 of human neuroserpin, with a histidine-to-arginine (H302R) exchange as the best modification to induce aggregation of SRP-2^{H302R} (Figure 2B). Another reason for choosing the disruptive H302R mutation was that milder neuroserpin mutations such as the S49P mutation develop FENIB much later in life, with detection of aggregates potentially exceeding life spans of short-lived organisms such

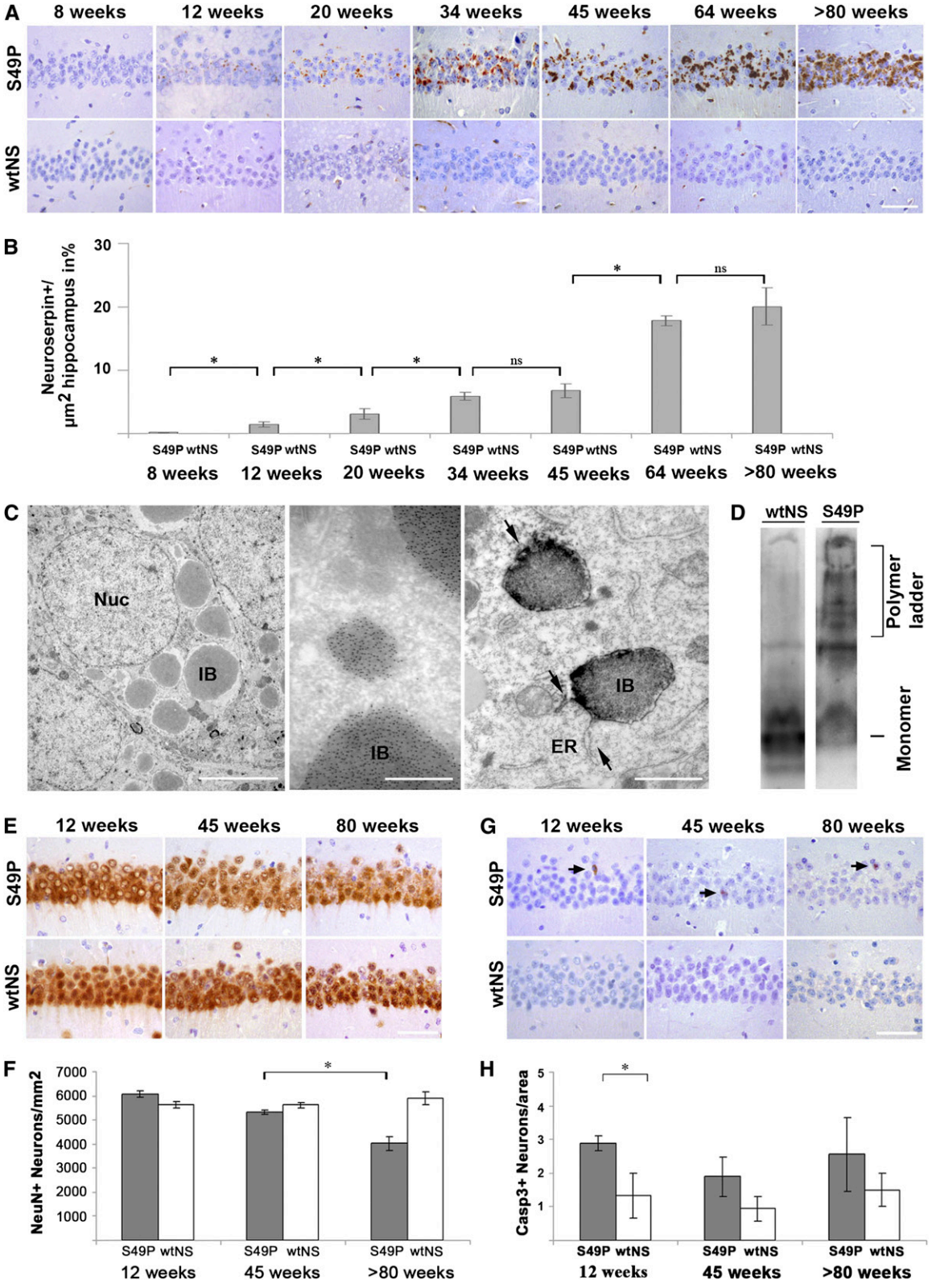

Figure 1 Accumulation of mutant neuroserpin in the ER correlates with neurodegeneration in FENIB mice. (A) Immunohistochemical staining for neuroserpin in CA1 and CA2 hippocampal regions of aged (8, 12, 20, 34, 45, 64, and >80 weeks) mice ($n = 4$). Neuroserpin accumulates progressively in *Tg*(NS^{S49P}) but not in *Tg*(NS) over time. (B) Quantification of sections shown in A. S49P neuroserpin aggregation reaches a temporary plateau from weeks 34 to 45 with an exponential rise at a later timepoint. (C) Electron micrographs from cortical neurons of >70-week-old *Tg*(NS^{S49P}) mice (left). Inclusion bodies (IBs) are found in the cytoplasm (Nuc, nucleus). IBs are positive in immunogold labeling for neuroserpin (IB, middle). In preembedding DAB-labeled tissue, neuroserpin positive IBs are found within rough ER (ER, right arrows). (D) Brain homogenates of 45-week-old *Tg*(NS^{S49P}) and *Tg*(NS)

as *C. elegans*. For visualization of the transgenic protein, YFP was fused to the C terminus of SRP-2. Transgenic lines expressing wild-type SRP-2 or SRP-2^{H302R} under the endogenous (*srp-2*::*srp-2*::*YFP*; *srp-2*::*srp-2^{H302R}*::*YFP*) or a muscle-specific (*unc-54*::*srp-2*::*YFP*; *unc-54*::*srp-2^{H302R}*::*YFP*) promoter were generated. These worms expressing SRP-2^{H302R} showed fluorescently labeled protein aggregates in the corresponding tissues (intestine and phasmid neurons or striated muscle) in an age-dependent manner (Figure 3A, Figure S2 and Figure S3). Aggregates are first detectable at L2 stage with most pronounced SRP-2 accumulation in young adults (Figure S1). Unlike previously described by Pak *et al.* (2004), we did not detect growth defects or developmental problems (Figure S4). This might be due to the lower copy number of our SRP-2 transgenes, which were integrated by biolistic transformation avoiding excessive overexpression (Praitis *et al.* 2001). To further define the nature of SRP-2 aggregates, we performed FRAP experiments for SRP-2^{H302R}, YFP, and polyQ-YFP expressed in body wall muscle cells (Morley *et al.* 2002; Brignull *et al.* 2006). In contrast to the wild-type protein, no obvious recovery was detectable for the mutant form (Figure 3, B and C), indicating that SRP-2^{H302R} forms insoluble polymers within cellular compartments. Polymer formation was confirmed by nondenaturing PAGE. Whereas wild-type SRP-2 runs predominantly as a single band, laddering of mutant SRP-2^{H302R} expressed from independent transgenic lines reflects polymeric aggregates of different size. We show this for two integrated (Is) and one extrachromosomal (Ex) line of either wild-type or mutant SRP-2 (Figure 3D).

To further investigate whether these aggregates interfere with cellular integrity, we compared the localization of fluorescently tagged SRP-2 with F-actin of muscle fibers. While wild-type SRP-2 colocalized with actin-myosin filaments, SRP-2^{H302R} accumulated adjacent to actin-myosin filaments (Figure 3E). Aggregation of mutant SRP-2^{H302R} was associated with decreased muscle motility as measured by counting body bends of worms (Figure 3F). These movement defects can be reduced by RNAi-mediated depletion of the YFP fusion protein, thus SRP-2^{H302R} aggregation seems to affect muscle function (Figure 3F). As a control for the experiments we use the established lines for YFP and Q40::YFP as previously described (Gidalevitz *et al.* 2009).

Defects in the UPR cause enhanced SRP-2 aggregation in worms

Since mutant neuroserpin accumulates in the ER of transgenic mice, we were interested to see whether SRP-2^{H302R} aggregates similarly in *C. elegans* (Galliciotti *et al.* 2007). Given the motility defect of worms expressing mutant SRP-2^{H302R} under the muscle-specific promoter, these transgenic worms were used for further analysis. Indeed, aggregated SRP-2^{H302R} accumulates around the nucleus, suggesting a related localization in the ER as shown for mutant neuroserpin in mice (Figure 1C and Figure 4A) (Galliciotti *et al.* 2007). It is known that ER accumulation of misfolded proteins leads to ER stress and induction of the UPR, although for serpins this requires a second insult (Hidvegi *et al.* 2005; Marciniak and Ron 2006; Davies *et al.* 2009). Therefore, we investigated the importance of different stress response pathways and monitored SRP-2^{H302R} aggregation in the absence of the central transcription factor HSF-1, regulating the heat shock response or one of the three different pathways of the UPR that require IRE-1, ATF-6, and PEK-1 (PERK in mammals), respectively. Genetic depletion of HSF-1 led to strong increase in aggregate formation of SRP-2^{H302R}, while inactivation of either branch of the ER stress response led to significant but less severe aggregation, with *pek-1* showing the most pronounced contribution (Figure 4, B and C). To further confirm these findings we used denaturing (Figure 4D, bottom) and nondenaturing (Figure 4D, top) PAGE to detect changes in the total level of mutant SRP-2 and the polymeric fraction. In line with the increased aggregate formation in muscle cells (Figure 4, B and C), the biochemical analysis of whole worm lysates suggests that loss of HSF-1 or PEK-1 activity causes an increase of polymeric SRP-2^{H302R} (Figure 4D, top), which is further reflected by increased total amounts (Figure 4D, bottom). Interestingly, we observed additive effects upon codepletion of *hsf-1* with *pek-1* or *ire-1*, resulting in significantly enhanced aggregation of SRP-2^{H302R} (Figure 4, E and F and Table S1). In contrast, ATF-6 activity seems to overlap with PEK-1, IRE-1, and HSF-1 function (Figure S6). Together, these results suggest that both cytosolic and ER quality control pathways might cooperate in proteostasis, modulating the aggregation of SRP-2^{H302R}.

Neuroserpin aggregation activates the UPR

As our analysis in worms provides evidence for the importance of ER stress pathways in modifying the formation of protein aggregates, we were interested in testing whether similar mechanisms exist in mammals. Therefore, we tested whether neuroserpin aggregation might correlate with the induction of ER stress markers in mice. ER stress causes activation of the PERK-, IRE1-, and ATF6-dependent pathways, which attenuate protein translation and induce chaperone expression to restore ER function (Ron and Walter 2007). Thus, we analyzed activation of the IRE1-mediated cleavage of XBP1 mRNA. We could detect processed forms of XBP1 mRNA in *Tg*(NS^{S49P}) and *Tg*(NS) mice at the

mice, analyzed by nondenaturating PAGE show mutant neuroserpin as a polymer ladder, wild-type neuroserpin as monomers. (E and G) Immunohistochemical stainings for NeuN and caspase-3 in the hippocampus of mice. (F and H) Quantification of sections shown in E and G. (F) NeuN positive neurons show substantial loss of neurons only in aged (45 and 80 weeks) *Tg*(NS^{S49P}) mice but not in *Tg*(NS) mice when compared to younger littermates (12 weeks). (H) Caspase-3 positive neurons show enhanced apoptosis in *Tg*(NS^{S49P}) mice. Bars, (A, E, and G) 50 μm; (C, left to right) 5 μm, 500 nm, and 1 μm. Statistical significance $^{*}P \leq 0.05$; NS $P \geq 0.05$.

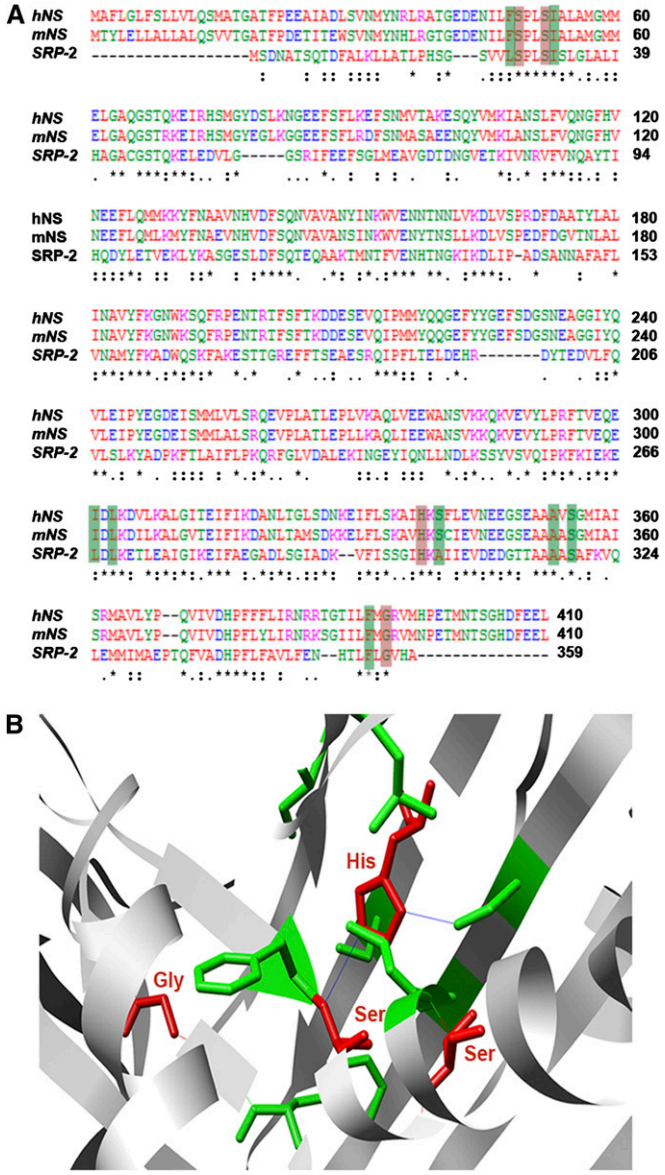

Figure 2 Comparison of neuroserpin and SRP-2. (A) Alignment of human (hNS) and mouse (mNS) neuroserpin with SRP-2. Sites causing FENIB are shadowed in red and amino acids forming a hydrophobic pocket in green (*, identical amino acids; : and ., amino acids with similar characteristics). (B) Structure of mouse neuroserpin showing close proximity of amino acids with disease-causing mutations (in red).

assessed timepoints (Figure 5A). Since this assay does not allow for quantitative analysis of XBP1 splicing, subtle differences pointing to a mutation-specific induction of this branch of the UPR could not be detected and presence of cleaved XBP1 mRNA in *Tg*(NS) mice is most likely due to neuroserpin overexpression (Calfon *et al.* 2002; Galliciotti *et al.* 2007). We next measured the presence of activated or cleaved ATF6 fragments and the phosphorylated form of eukaryotic initiation factor 2 alpha (eIF2alphaP, as a PERK-dependent signal). Expression of cleaved ATF6 peaked in mutant neuroserpin mice between 34 and 45 weeks (Figure 5, B and C), whereas eIF2alphaP was highest in *Tg*(NS^{S49P}) mice at 20 weeks of age when compared to wild-type mice (Figure 5, D and E). This argues for an age-dependent selective and temporally limited activation of two different ER stress pathways in *Tg*(NS^{S49P}). The availability of an ELISA specific for polymeric neuroserpin (Miranda *et al.* 2008) allowed us to investigate the temporal distribution of polymeric neuroserpin in *Tg*(NS^{S49P}) and *Tg*(NS) mice. This analysis revealed a temporary decline of polymeric neuroserpin between weeks 20 and 45 and an exponential increase from week 64 onwards in *Tg*(NS^{S49P}), whereas polymeric neuroserpin could not be detected in *Tg*(NS) at any timepoint (Figure 5F). This is partially paralleled by a slight decrease of total neuroserpin from week 12 to week 34 and a subsequent exponential increase in total neuroserpin in *Tg*(NS^{S49P}), with a constant and low level of total neuroserpin in *Tg*(NS) (Figure 5G).

In summary, our data support the idea that the accumulation of mutant SRP-2 is sensitive to perturbation of cytosolic or ER proteostasis in the worm, which nicely correlates with the observation that partial activation of the UPR reduced the formation of mutant neuroserpin polymers in FENIB mice.

Discussion

Dementias are typically associated with the deposition of nonnative aggregated proteins (Lomas and Carrell 2002). Usually, protein aggregation is caused by aberrant protein interactions resulting in intracellular or extracellular deposits. Recently, the concept of neuronal proteostasis has been postulated, which explains the integrity of intracellular proteins regulated by quality control pathways that influence protein synthesis, folding, disaggregation, and degradation (Garcia *et al.* 2007; Balch *et al.* 2008). For example, secretory and ER resident proteins are specifically controlled by the UPR and ERAD (Schroder and Kaufman 2005). In certain dementias, intracellular protein accumulation seems to be involved in disease pathophysiology, yet the role of the UPR in protein aggregation and disease progression is unclear. Here we studied the importance of proteostasis in *C. elegans* and murine models of the conformational dementia FENIB, where aberrantly folded neuroserpin accumulates within the ER lumen causing neurodegeneration. FENIB is well suited as a model disease to study how ER dysfunction, ERAD, and protein aggregation are linked, since the entire disease pathophysiology is dictated by mutation-specific accumulation of a single protein in the ER, and mouse models fully recapitulate the human disease (Galliciotti *et al.* 2007; Takasawa *et al.* 2008). Our work extends these analyses and clearly shows ER localization of mutant neuroserpin and prominent neurodegeneration with the involvement of apoptotic pathways. The *C. elegans* model we established here differs from others, where chimeric polyQ stretches or human aggregation-prone proteins are expressed, by choosing an endogenous homolog to introduce disease-causing mutations (Link 1995; Cooper *et al.* 2006; van Ham *et al.* 2008; Brandt *et al.* 2009; Markaki and Tavernarakis 2010). Besides

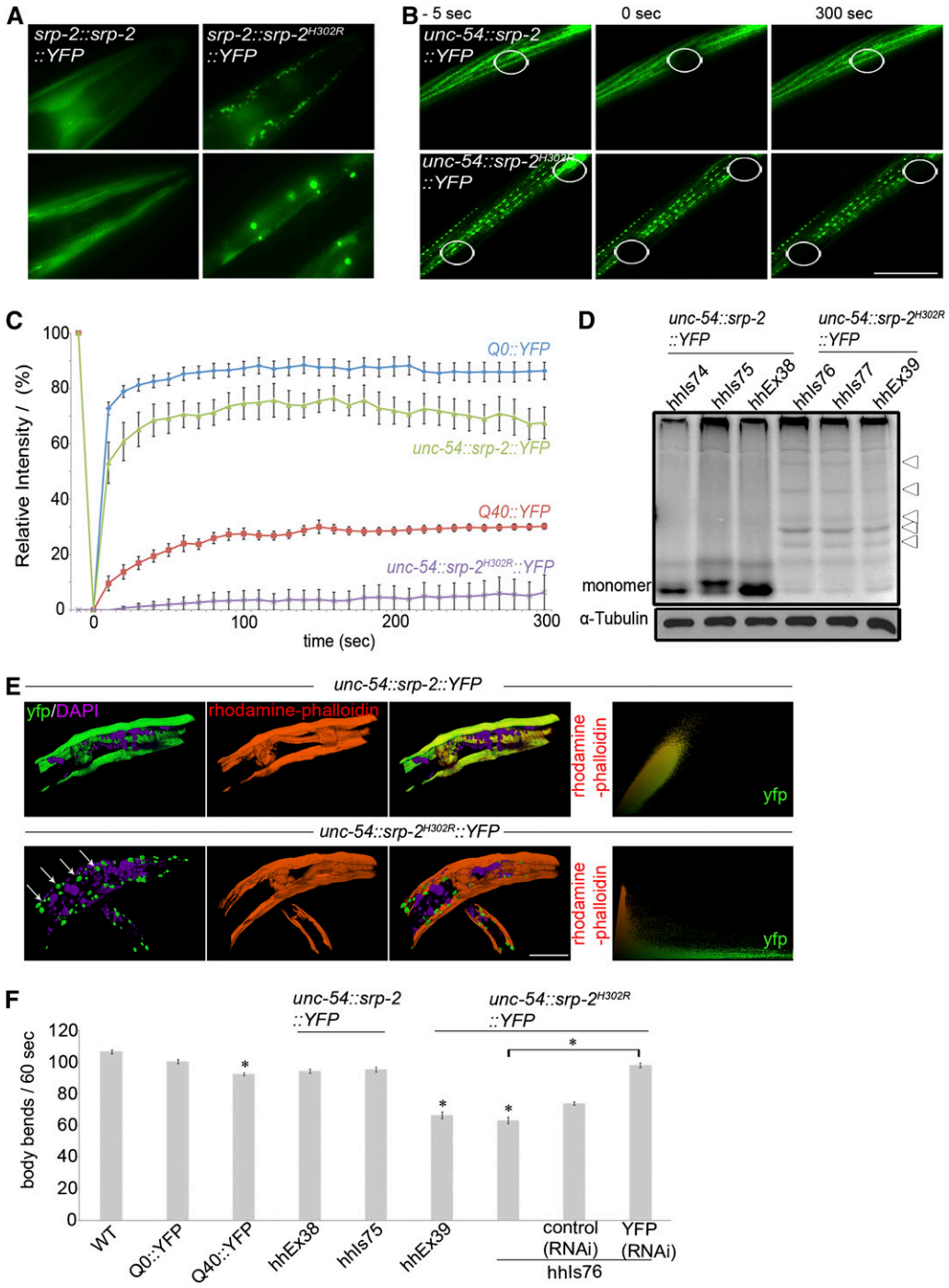

Figure 3 SRP-2^{H302R} forms immobile protein aggregates in muscle cells leading to movement defects of transgenic worms. (A) In contrast to SRP-2 (wild-type), SRP-2^{H302R} forms protein aggregates when expressed under its own and muscle-specific promoter. (B) Fluorescent images of representative FRAP experiments (B) and their graphic demonstration (C) show efficient fluorescence recovery of SRP-2 but not SRP-2^{H302R}. SRP-2 (light green) shows slightly less fluorescence recovery than Q0::YFP (as control lacking inclusions, blue), whereas FRAP of SRP-2^{H302R} (purple) is comparable to Q40::YFP (as control expressing 40 repeats of fluorescently tagged polyQ proteins with considerable inclusions, red). The traces are averages of five or more replicates (n = 7). (D, upper panel) 7.5 % native PAGE of extracts from indicated strains. SRP-2^{H302R} (two independent integrated lines, *hhls76*, *hhls77*, and one extrachromosomal line *hhEx39*) forms high molecular weight aggregates (lanes 4 to 6) whereas SRP-2 (two independent integrated lines, *hhls74*, *hhls75*, and one extrachromosomal line, *hhEx39*, lanes 1 to 3) runs as a single band. Lower panel: SDS-Page to quantify tubulin for equal loading. (E) Confocal projections of transgenic worms showing the distribution of YFP–SRP-2 (green) and rhodamine-phalloidin that stained myofilaments (red). SRP-2 colocalizes with F-actin protein as shown by scatterplot, while SRP-2^{H302R} deposits as discrete fluorescent foci that do not disrupt the myofilament structure. (F) Body bends of worms (lines as described in D) per minute were measured. (n = 30) Bars, (A, B, and E) 50 μm. Statistical significance *$P \leq 0.05$; NS $P \geq 0.05$.

using the well-characterized promoter *unc-54* (Morley *et al.* 2002) leading to expression in striated muscle, we have additionally expressed mutant SRP-2^{H302R} and wild-type SRP-2 under its endogenous promoter. Morphological and behavioral analysis of transgenic worms demonstrated aged-dependent deposition of SRP-2^{H302R} causing movement defects. Interestingly, these defects are associated with the presence of polymeric forms of SRP-2 in intracellular aggregates. Thus, our model nicely extends the existing repertoire of *C. elegans* aggregation approaches and shows that a carefully chosen single point mutation in a worm-encoded gene can phenocopy aggregation of the human homolog. Unlike other proteins that spontaneously accumulate in aged *C. elegans* (*i.e.*, KIN-19 or RHO-1), SRP-2 only accumulates when specific disease-associated mutations are introduced (David *et al.* 2010). Since neuroserpin and SRP-2 aggregate within the ER lumen, we explored the relationship between protein aggregation and the UPR response. Interestingly, genetic disruption of

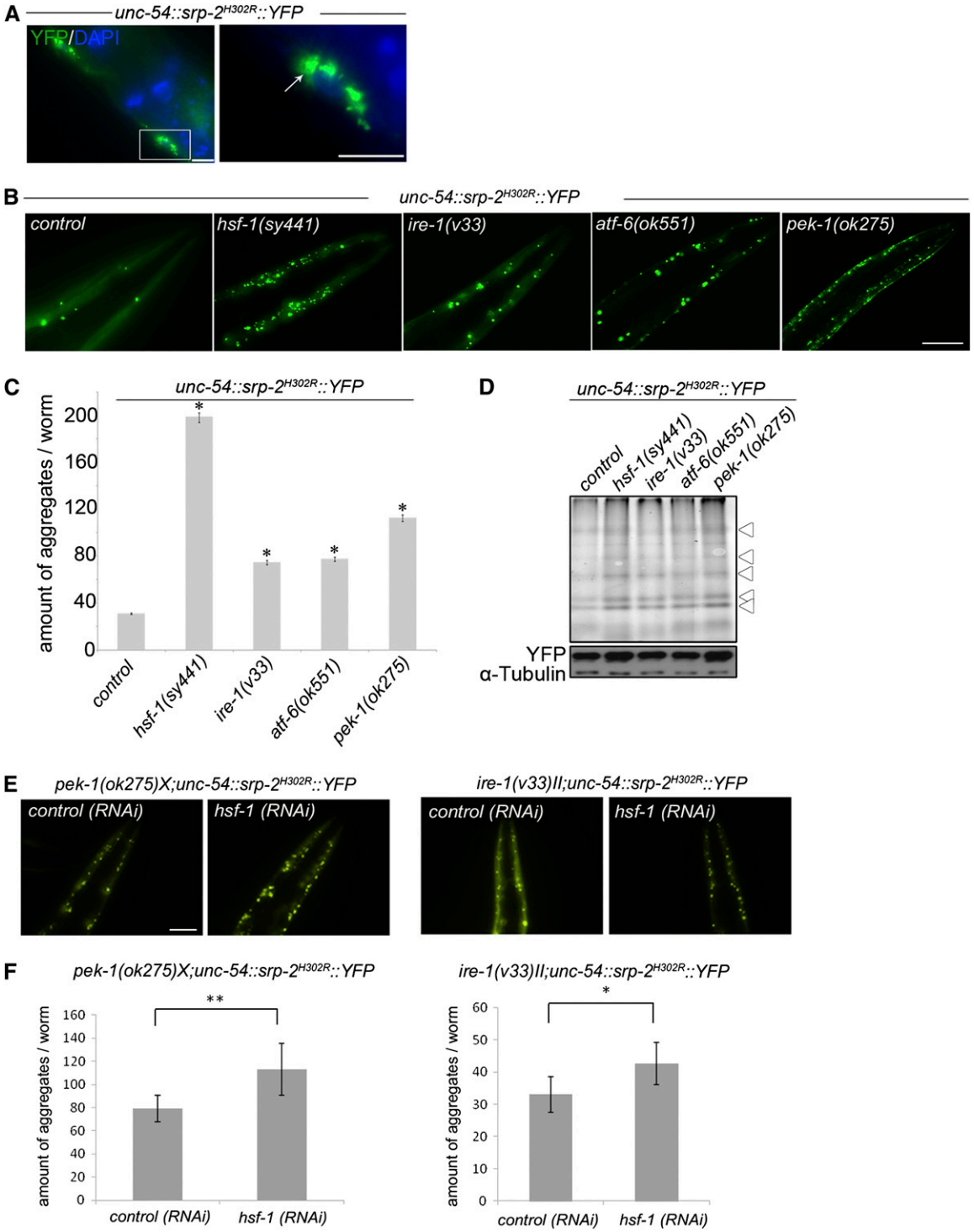

Figure 4 Genetic deletion of HSF-1 and UPR pathways increase the amount of SRP-2^{H302R} aggregates. (A) Fluorescent image of SRP-2^{H302R} shows perinuclear localization consistent with ER localization (DAPI staining; right picture is a close-up of the merged image). (B) Representative fluorescent images of mutants lacking *hsf-1*, *ire-1*, *atf-6*, and *pek-1*. (C) Quantification of aggregates of SRP-2^{H302R} worms described in B (n = 15). (D) Native and denaturing PAGE of extracts from indicated strains. Top native gel shows polymeric forms of SRP-2^{H302R}; bottom denaturing gel shows the total level of SRP-2^{H302R} probed with α-YFP antibodies. Tubulin was used as loading control. Integrated transgenic line *hhIs76* was used for B–D. (E) Representative fluorescent images of mutant worms lacking either *pek-1* or *ire-1* after inactivation of *hsf-1* for 48 hr by RNAi. The empty RNAi feeding vector pPD129.36 served as negative control. (F) Quantification of SRP-2^{H302R} aggregates described in E (n = 25). Bars, (A) 10 μm, (B and E) 50 μm. Statistical significance $*P \leq 0.05$; $**P \leq 0.01$ (two-tailed Student's t-test).

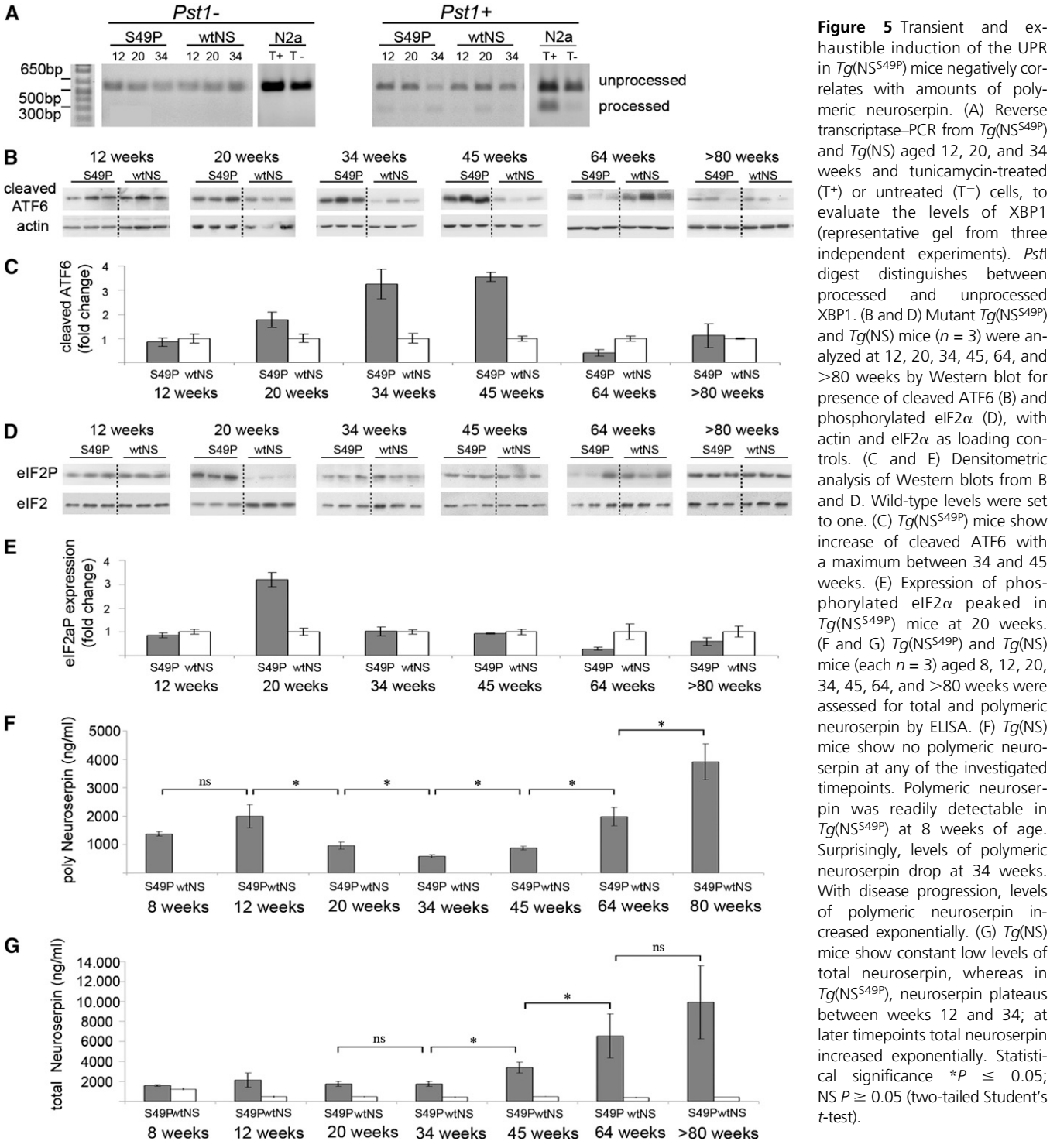

Figure 5 Transient and exhaustible induction of the UPR in *Tg*(NS^{S49P}) mice negatively correlates with amounts of polymeric neuroserpin. (A) Reverse transcriptase–PCR from *Tg*(NS^{S49P}) and *Tg*(NS) aged 12, 20, and 34 weeks and tunicamycin-treated (T^+) or untreated (T^-) cells, to evaluate the levels of XBP1 (representative gel from three independent experiments). *Pst*I digest distinguishes between processed and unprocessed XBP1. (B and D) Mutant *Tg*(NS^{S49P}) and *Tg*(NS) mice ($n = 3$) were analyzed at 12, 20, 34, 45, 64, and >80 weeks by Western blot for presence of cleaved ATF6 (B) and phosphorylated eIF2α (D), with actin and eIF2α as loading controls. (C and E) Densitometric analysis of Western blots from B and D. Wild-type levels were set to one. (C) *Tg*(NS^{S49P}) mice show increase of cleaved ATF6 with a maximum between 34 and 45 weeks. (E) Expression of phosphorylated eIF2α peaked in *Tg*(NS^{S49P}) mice at 20 weeks. (F and G) *Tg*(NS^{S49P}) and *Tg*(NS) mice (each $n = 3$) aged 8, 12, 20, 34, 45, 64, and >80 weeks were assessed for total and polymeric neuroserpin by ELISA. (F) *Tg*(NS) mice show no polymeric neuroserpin at any of the investigated timepoints. Polymeric neuroserpin was readily detectable in *Tg*(NS^{S49P}) at 8 weeks of age. Surprisingly, levels of polymeric neuroserpin drop at 34 weeks. With disease progression, levels of polymeric neuroserpin increased exponentially. (G) *Tg*(NS) mice show constant low levels of total neuroserpin, whereas in *Tg*(NS^{S49P}), neuroserpin plateaus between weeks 12 and 34; at later timepoints total neuroserpin increased exponentially. Statistical significance $^*P \leq 0.05$; NS $P \geq 0.05$ (two-tailed Student's *t*-test).

all three branches of the UPR or central chaperones led to increase in both deposited and polymeric forms of SRP-2 in worms. However, an even more dramatic effect was seen following perturbation of the cytosolic heat shock response, arguing that serpin accumulation is sensitive to defects in general proteostasis. Having shown that impaired proteostasis can exacerbate protein deposition in worms, we looked for activation of the UPR in our murine FENIB model. These data demonstrate an age-dependent activation of ATF6 and PERK, whereas we could not detect IRE1 induction in mice expressing mutant neuroserpin. Beneficial effects of active ATF6 in the clearance of serpin polymers have recently been shown in cells thus supporting our finding of selective UPR activity (Smith *et al.* 2011). The induction of all three branches of the UPR is controversial for serpinopathies, with several reports showing absence (Davies *et al.* 2009; Kroeger *et al.*

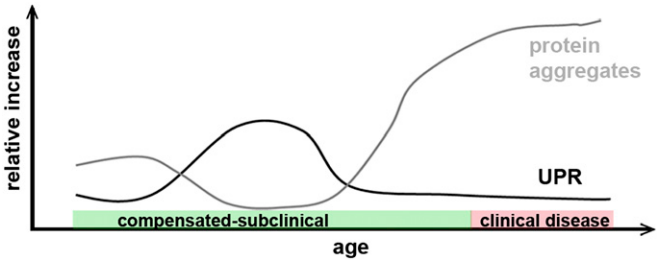

Figure 6 Hypothetical model how transient UPR induction and aggregation-prone proteins are interconnected in conformational dementia. In our proposed model, transient induction of the UPR in young mice limits polymer formation. With increasing age, these mechanisms cease resulting in an exponential increase of protein aggregates. Increase in aggregates (present as polymers and potentially in equilibrium with oligomers) cosegregates with neurodegeneration and clinical disease develops once the functional reserve capacity of the CNS is exhausted.

2009) or presence of the UPR (Lawless *et al.* 2004). Instead, an ER stress response distinct from classical UPR signaling has been reported (Davies *et al.* 2009). The transient, age-dependent induction of the UPR suggests the necessity of a second insult, possibly aging, to mount an UPR response. This finding unifies current concepts of disturbed proteostasis in FENIB (Lawless *et al.* 2004; Hidvegi *et al.* 2005; Davies *et al.* 2009). Since IRE1 signaling has been linked to autophagy, the relatively low induction of IRE1 signaling in our murine FENIB model may help to explain the fact that autophagy is only mildly increased in FENIB (Hetz *et al.* 2009; Kroeger *et al.* 2009). Other than the serpinopathies, ER stress has been shown to be prominently involved in the pathophysiology of other dementias with intracellular protein accumulation (Hoozemans *et al.* 2009; Salminen *et al.* 2009). ERAD and the UPR are coregulated and the recently demonstrated involvement of ERAD in the degradation of mutant neuroserpin further underscores the tight integration of the proteostasis machinery (Kroeger *et al.* 2009; Ying *et al.* 2011). The mechanistic importance of ERAD is further extended by our data showing a fundamental role of HSF-1 in controlling SRP-2^{H302R} accumulation, further supporting the idea that HSF-1 might be linked to ERAD and UPR (Liu and Chang 2008). Intriguingly, our data demonstrate that transient stimulation of the UPR decreases neuroserpin polymer formation only in younger mice and probably age-related decline of ER quality control results in an exponential increase of neuroserpin polymers causing neurodegeneration (Figure 6). The fact that dementias show age-specific distribution and exponential rise of incidence with age argues in favor of age-specific phenomena perturbing neuronal protein homeostasis (Rubinsztein 2006; Salminen *et al.* 2010). Our data suggest that protein aggregation is tightly regulated by proteostasis pathways such as the UPR and ERAD, which seem to be modified by additional stressors accumulating with age. Future studies will further clarify whether ER stress pathways are specific for dementias with intracellular protein depositions, such as FENIB, or are also generally important for extracellular protein aggregation.

Acknowledgments

We thank S. J. Marciniak, P. Sonderegger, A. Fire, R. Morimoto, L. Neukomm, Cliff J. Luke, the Caenorhabditis Genetics Center, the Dana-Farber Cancer Institute, and Geneservice for antibodies, plasmids, cDNAs, and strains. This work is supported by grants from the Deutsche Forschungsgemeinschaft (especially the FOR885 to M.G. and T.H., the Cologne Excellence Cluster on Cellular Stress Responses in Aging-Associated Diseases to T. H. and GRK1459 to M.G), the Medical Research Council (United Kingdom) to D.L., the Hans und Ilse Breuer Foundation to S.L., the Leibniz Center Infection graduate school (model systems for infectious diseases), and the Landesexzellenzinitiative of Hamburg to M.G.

Literature Cited

Balch, W. E., R. I. Morimoto, A. Dillin, and J. W. Kelly, 2008 Adapting proteostasis for disease intervention. Science 319: 916–919.

Borges, V. M., T. W. Lee, D. L. Christie, and N. P. Birch, 2010 Neuroserpin regulates the density of dendritic protrusions and dendritic spine shape in cultured hippocampal neurons. J. Neurosci. Res. 88: 2610–2617.

Brandt, R., A. Gergou, I. Wacker, T. Fath, and H. Hutter, 2009 A Caenorhabditis elegans model of tau hyperphosphorylation: induction of developmental defects by transgenic overexpression of Alzheimer's disease-like modified tau. Neurobiol. Aging 30: 22–33.

Brenner, S., 1974 The genetics of Caenorhabditis elegans. Genetics 77: 71–94.

Brignull, H. R., F. E. Moore, S. J. Tang, and R. I. Morimoto, 2006 Polyglutamine proteins at the pathogenic threshold display neuron-specific aggregation in a pan-neuronal Caenorhabditis elegans model. J. Neurosci. 26: 7597–7606.

Calfon, M., H. Zeng, F. Urano, J. H. Till, S. R. Hubbard *et al.*, 2002 IRE1 couples endoplasmic reticulum load to secretory capacity by processing the XBP-1 mRNA. Nature 415: 92–96.

Chakrabarti, A., A. W. Chen, and J. D. Varner, 2011 A review of the mammalian unfolded protein response. Biotechnol. Bioeng. 108: 2777–2793.

Cooper, A. A., A. D. Gitler, A. Cashikar, C. M. Haynes, K. J. Hill *et al.*, 2006 Alpha-synuclein blocks ER-Golgi traffic and Rab1 rescues neuron loss in Parkinson's models. Science 313: 324–328.

David, D. C., N. Ollikainen, J. C. Trinidad, M. P. Cary, A. L. Burlingame *et al.*, 2010 Widespread protein aggregation as an inherent part of aging in C. elegans. PLoS Biol. 8: e1000450.

Davies, M. J., E. Miranda, B. D. Roussel, R. J. Kaufman, S. J. Marciniak *et al.*, 2009 Neuroserpin polymers activate NF-{kappa}B by a calcium signaling pathway that is independent of the unfolded protein response. J. Biol. Chem. 284: 18202–18209.

Davis, R. L., A. E. Shrimpton, P. D. Holohan, C. Bradshaw, D. Feiglin *et al.*, 1999 Familial dementia caused by polymerization of mutant neuroserpin. Nature 401: 376–379.

Davis, R. L., A. E. Shrimpton, R. W. Carrell, D. A. Lomas, L. Gerhard *et al.*, 2002 Association between conformational mutations in neuroserpin and onset and severity of dementia. Lancet 359: 2242–2247.

Galliciotti, G., M. Glatzel, J. Kinter, V. K. Kozlov, P. Cinelli *et al.*, 2007 Accumulation of mutant Neuroserpin precedes development of clinical symptoms in familial encephalopathy with neuroserpin inclusion bodies. Am. J. Pathol. 170: 1305–1313.

Garcia, S. M., M. O. Casanueva, M. C. Silva, M. D. Amaral, and R. I. Morimoto, 2007 Neuronal signaling modulates protein homeostasis

in Caenorhabditis elegans post-synaptic muscle cells. Genes Dev. 21: 3006–3016.
Gidalevitz, T., T. Krupinski, S. Garcia, and R. I. Morimoto, 2009 Destabilizing protein polymorphisms in the genetic background direct phenotypic expression of mutant SOD1 toxicity. PLoS Genet. 5: e1000399.
Glatzel, M., F. L. Heppner, K. M. Albers, and A. Aguzzi, 2001 Sympathetic innervation of lymphoreticular organs is rate limiting for prion neuroinvasion. Neuron 31: 25–34.
Hagen, M. C., J. R. Murrell, M. B. Delisle, E. Andermann, F. Andermann *et al.*, 2011 Encephalopathy with neuroserpin inclusion bodies presenting as progressive myoclonus epilepsy and associated with a novel mutation in the proteinase inhibitor 12 gene. Brain Pathol. 21: 575–582.
Hetz, C., P. Thielen, S. Matus, M. Nassif, F. Court *et al.*, 2009 XBP-1 deficiency in the nervous system protects against amyotrophic lateral sclerosis by increasing autophagy. Genes Dev. 23: 2294–2306.
Hidvegi, T., B. Z. Schmidt, P. Hale, and D. H. Perlmutter, 2005 Accumulation of mutant alpha1-antitrypsin Z in the endoplasmic reticulum activates caspases-4 and -12, NFkappaB, and BAP31 but not the unfolded protein response. J. Biol. Chem. 280: 39002–39015.
Hoozemans, J. J., E. S. van Haastert, D. A. Nijholt, A. J. Rozemuller, P. Eikelenboom *et al.*, 2009 The unfolded protein response is activated in pretangle neurons in Alzheimer's disease hippocampus. Am. J. Pathol. 174: 1241–1251.
Kamath, R. S., M. Martinez-Campos, P. Zipperlen, A. G. Fraser, and J. Ahringer, 2001 Effectiveness of specific RNA-mediated interference through ingested double-stranded RNA in Caenorhabditis elegans. Genome Biol. 2: 1–10.
Kikis, E. A., T. Gidalevitz, and R. I. Morimoto, 2010 Protein homeostasis in models of aging and age-related conformational disease. Adv. Exp. Med. Biol. 694: 138–159.
Kroeger, H., E. Miranda, I. Macleod, J. Perez, D. C. Crowther *et al.*, 2009 ERAD and autophagy cooperate to degrade polymerogenic mutant serpins. J. Biol. Chem. 21: 22793–22802.
Lappe-Siefke, C., S. Loebrich, W. Hevers, O. B. Waidmann, M. Schweizer *et al.*, 2009 The ataxia (axJ) mutation causes abnormal GABAA receptor turnover in mice. PLoS Genet. 5: e1000631.
Lawless, M. W., C. M. Greene, A. Mulgrew, C. C. Taggart, S. J. O'Neill *et al.*, 2004 Activation of endoplasmic reticulum-specific stress responses associated with the conformational disease Z alpha 1-antitrypsin deficiency. J. Immunol. 172: 5722–5726.
Link, C. D., 1995 Expression of human beta-amyloid peptide in transgenic Caenorhabditis elegans. Proc. Natl. Acad. Sci. USA 92: 9368–9372.
Liu, Y., and A. Chang, 2008 Heat shock response relieves ER stress. EMBO J. 27: 1049–1059.
Lomas, D. A., and R. W. Carrell, 2002 Serpinopathies and the conformational dementias. Nat. Rev. Genet. 3: 759–768.
Luke, C. J., S. C. Pak, D. J. Askew, Y. S. Askew, J. E. Smith *et al.*, 2006 Selective conservation of the RSL-encoding, proteinase inhibitory-type, clade L serpins in Caenorhabditis species. Front. Biosci. 11: 581–594.
Marciniak, S. J., and D. Ron, 2006 Endoplasmic reticulum stress signaling in disease. Physiol. Rev. 86: 1133–1149.
Markaki, M., and N. Tavernarakis, 2010 Modeling human diseases in Caenorhabditis elegans. Biotechnol. J. 5: 1261–1276.
McIntire, S. L., G. Garriga, J. White, D. Jacobson, and H. R. Horvitz, 1992 Genes necessary for directed axonal elongation or fasciculation in C. elegans. Neuron 8: 307–322.
Miedel, M. T., N. J. Graf, K. E. Stephen, O. S. Long, S. C. Pak *et al.*, 2012 A pro-cathepsin L mutant is a luminal substrate for endoplasmic-reticulum-associated degradation in C. elegans. PLoS ONE 7: e40145.
Miranda, E., I. MacLeod, M. J. Davies, J. Perez, K. Romisch *et al.*, 2008 The intracellular accumulation of polymeric neuroserpin explains the severity of the dementia FENIB. Hum. Mol. Genet. 17: 1527–1539.
Miranda, E., K. Romisch, and D. A. Lomas, 2004 Mutants of neuroserpin that cause dementia accumulate as polymers within the endoplasmic reticulum. J. Biol. Chem. 279: 28283–28291.
Morley, J. F., H. R. Brignull, J. J. Weyers, and R. I. Morimoto, 2002 The threshold for polyglutamine-expansion protein aggregation and cellular toxicity is dynamic and influenced by aging in Caenorhabditis elegans. Proc. Natl. Acad. Sci. USA 99: 10417–10422.
Nollen, E. A., S. M. Garcia, G. van Haaften, S. Kim, A. Chavez *et al.*, 2004 Genome-wide RNA interference screen identifies previously undescribed regulators of polyglutamine aggregation. Proc. Natl. Acad. Sci. USA 101: 6403–6408.
Nonet, M. L., K. Grundahl, B. J. Meyer, and J. B. Rand, 1993 Synaptic function is impaired but not eliminated in C. elegans mutants lacking synaptotagmin. Cell 73: 1291–1305.
Pak, S. C., V. Kumar, C. Tsu, C. J. Luke, Y. S. Askew *et al.*, 2004 SRP-2 is a cross-class inhibitor that participates in postembryonic development of the nematode Caenorhabditis elegans: initial characterization of the clade L serpins. J. Biol. Chem. 279: 15448–15459.
Praitis, V., E. Casey, D. Collar, and J. Austin, 2001 Creation of low-copy integrated transgenic lines in Caenorhabditis elegans. Genetics 157: 1217–1226.
Ron, D., and P. Walter, 2007 Signal integration in the endoplasmic reticulum unfolded protein response. Nat. Rev. Mol. Cell Biol. 8: 519–529.
Rubinsztein, D. C., 2006 The roles of intracellular protein-degradation pathways in neurodegeneration. Nature 443: 780–786.
Salminen, A., A. Kauppinen, T. Suuronen, K. Kaarniranta, and J. Ojala, 2009 ER stress in Alzheimer's disease: a novel neuronal trigger for inflammation and Alzheimer's pathology. J. Neuroinflammation 6: 41.
Salminen, A., A. Kauppinen, J. M. Hyttinen, E. Toropainen, and K. Kaarniranta, 2010 Endoplasmic reticulum stress in age-related macular degeneration: trigger for neovascularization. Mol. Med. 16: 535–542.
Schroder, M., and R. J. Kaufman, 2005 The mammalian unfolded protein response. Annu. Rev. Biochem. 74: 739–789.
Sepulveda-Falla, D., J. Matschke, C. Bernreuther, C. Hagel, B. Puig *et al.*, 2011 Deposition of hyperphosphorylated Tau in cerebellum of PS1 E280A Alzheimer's disease. Brain Pathol. 21: 452–463.
Slot, J. W., and H. J. Geuze, 2007 Cryosectioning and immunolabeling. Nat. Protoc. 2: 2480–2491.
Smith, S. E., S. Granell, L. Salcedo-Sicilia, G. Baldini, G. Egea *et al.*, 2011 Activating transcription factor 6 limits intracellular accumulation of mutant alpha-1-antitrypsin Z and mitochondrial damage in hepatoma cells. J. Biol. Chem. 286: 41563–41577.
Takasawa, A., I. Kato, K. Takasawa, Y. Ishii, T. Yoshida *et al.*, 2008 Mutation-, aging-, and gene dosage-dependent accumulation of neuroserpin (G392E) in endoplasmic reticula and lysosomes of neurons in transgenic mice. J. Biol. Chem. 283: 35606–35613.
Thelen, M., M. Damme, M. Schweizer, C. Hagel, A. M. Wong *et al.*, 2012 Disruption of the autophagy-lysosome pathway is involved in neuropathology of the nclf mouse model of neuronal ceroid lipofuscinosis. PLoS ONE 7: e35493.
Timmons, L., and A. Fire, 1998 Specific interference by ingested dsRNA. Nature 395: 854.
van Ham, T. J., K. L. Thijssen, R. Breitling, R. M. Hofstra, R. H. Plasterk *et al.*, 2008 C. elegans model identifies genetic modifiers of alpha-synuclein inclusion formation during aging. PLoS Genet. 4: e1000027.
van Ham, T. J., A. Esposito, J. R. Kumita, S. T. Hsu, G. S. Kaminski Schierle *et al.*, 2010 Towards multiparametric fluorescent im-

aging of amyloid formation: studies of a YFP model of alpha-synuclein aggregation. J. Mol. Biol. 395: 627–642.
Wu, J., R. Echeverry, J. Guzman, and M. Yepes, 2010 Neuroserpin protects neurons from ischemia-induced plasmin-mediated cell death independently of tissue-type plasminogen activator inhibition. Am. J. Pathol. 177: 2576–2584.
Ying, Z., H. Wang, H. Fan, and G. Wang, 2011 The endoplasmic reticulum (ER)-associated degradation system regulates aggregation and degradation of mutant neuroserpin. J. Biol. Chem. 286: 20835–20844.

Communicating editor: O. Hobert

GENETICS

Supporting Information
http://www.genetics.org/lookup/suppl/doi:10.1534/genetics.112.149088/-/DC1

A Novel Interaction Between Aging and ER Overload in a Protein Conformational Dementia

Angela Schipanski, Sascha Lange, Alexandra Segref, Aljona Gutschmidt, David A. Lomas, Elena Miranda, Michaela Schweizer, Thorsten Hoppe, and Markus Glatzel

DOI: 10.1534/genetics.112.149088

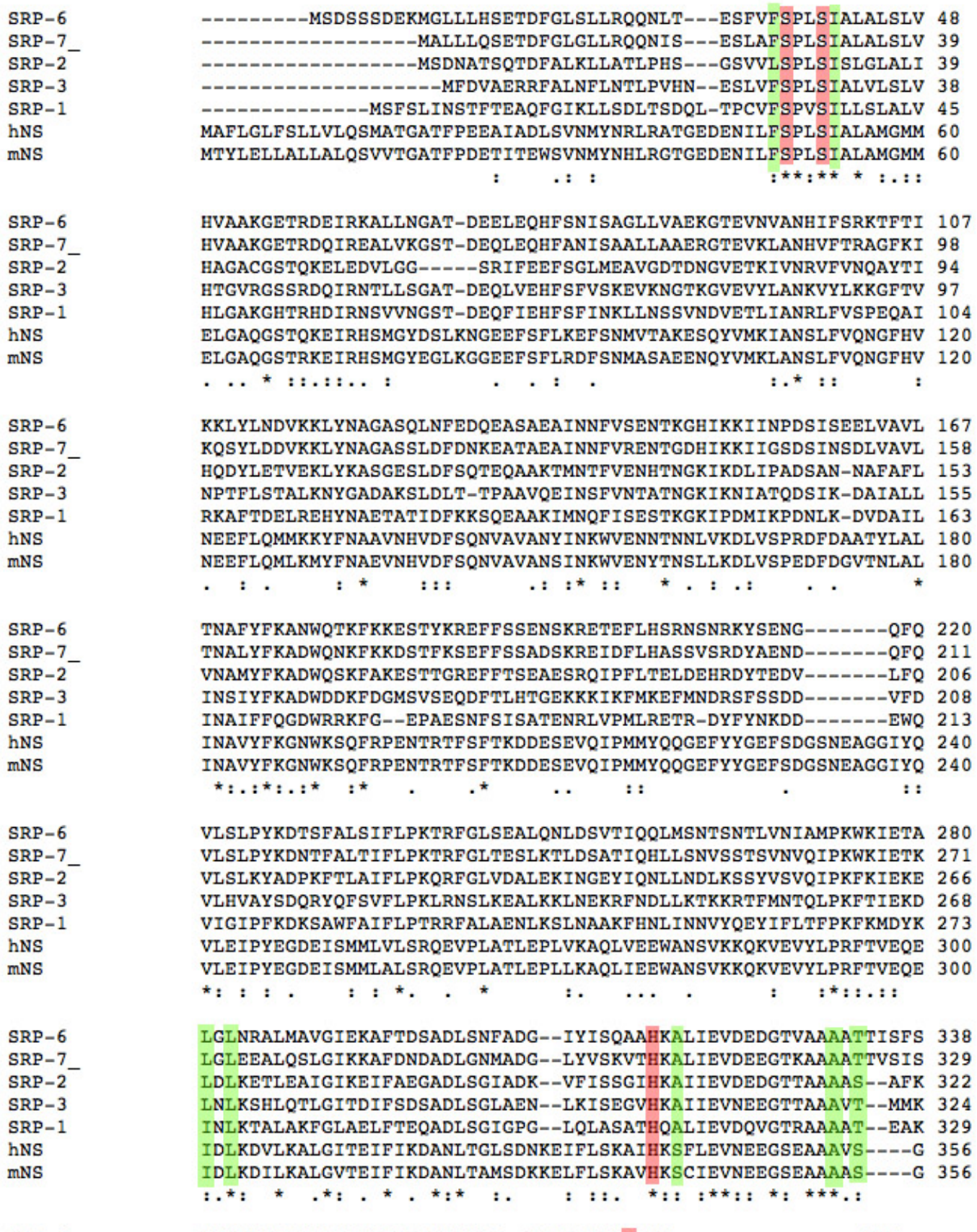
SRP-6 ---------MSDSSSDEKMGLLLHSETDFGLSLLRQQNLT---ESFVFSPLSIALALSLV 48
SRP-7_ ----------------MALLLQSETDFGLGLLRQQNIS---ESLAFSPLSIALALSLV 39
SRP-2 ----------------MSDNATSQTDFALKLLATLPHS---GSVVLSPLSISLGLALI 39
SRP-3 -------------------MFDVAERRFALNFLNTLPVHN--ESLVFSPLSIALVLSLV 38
SRP-1 -------------MSFSLINSTFTEAQFGIKLLSDLTSDQL-TPCVFSPVSILLSLALV 45
hNS MAFLGLFSLLVLQSMATGATFPEEAIADLSVNMYNRLRATGEDENILFSPLSIALAMGMM 60
mNS MTYLELLALLALQSVVTGATFPDETITEWSVNMYNHLRGTGEDENILFSPLSIALAMGMM 60
HVAAKGETRDEIRKALLNGAT-DEELEQHFSNISAGLLVAEKGTEVNVANHIFSRKTFTI 107
SRP-7_ HVAAKGETRDQIREALVKGST-DEQLEQHFANISAALLAAERGTEVKLANHVFTRAGFKI 98
SRP-2 HAGACGSTQKELEDVLGG-----SRIFEEFSGLMEAVGDTDNGVETKIVNRVFVNQAYTI 94
SRP-3 HTGVRGSSRDQIRNTLLSGAT-DEQLVEHFSFVSKEVKNGTKGVEVYLANKVYLKKGFTV 97
SRP-1 HLGAKGHTRHDIRNSVVNGST-DEQFIEHFSFINKLLNSSVNDVETLIANRLFVSPEQAI 104
hNS ELGAQGSTQKEIRHSMGYDSLKNGEEFSFLKEFSNMVTAKESQYVMKIANSLFVQNGFHV 120
mNS ELGAQGSTRKEIRHSMGYEGLKGGEEFSFLRDFSNMASAEENQYVMKLANSLFVQNGFHV 120
KKLYLNDVKKLYNAGASQLNFEDQEASAEAINNFVSENTKGHIKKIINPDSISEELVAVL 167
SRP-7_ KQSYLDDVKKLYNAGASSLDFDNKEATAEAINNFVRENTGDHIKKIIGSDSINSDLVAVL 158
SRP-2 HQDYLETVEKLYKASGESLDFSQTEQAAKTMNTFVENHTNGKIKDLIPADSAN-NAFAFL 153
SRP-3 NPTFLSTALKNYGADAKSLDLT-TPAAVQEINSFVNTATNGKIKNIATQDSIK-DAIALL 155
SRP-1 RKAFTDELREHYNAETATIDFKKSQEAAKIMNQFISESTKGKIPDMIKPDNLK-DVDAIL 163
hNS NEEFLQMMKKYFNAAVNHVDFSQNVAVANYINKWVENNTNNLVKDLVSPRDFDAATYLAL 180
mNS NEEFLQMLKMYFNAEVNHVDFSQNVAVANSINKWVENYTNSLLKDLVSPEDFDGVTNLAL 180
TNAFYFKANWQTKFKKESTYKREFFSSENSKRETEFLHSRNSNRKYSENG-------QFQ 220
SRP-7_ TNALYFKADWQNKFKKDSTFKSEFFSSADSKREIDFLHASSVSRDYAEND-------QFQ 211
SRP-2 VNAMYFKADWQSKFAKESTTGREFFTSEAESRQIPFLTELDEHRDYTEDV-------LFQ 206
SRP-3 INSIYFKADWDDKFDGMSVSEQDFTLHTGEKKKIKFMKEFMNDRSFSSDD-------VFD 208
SRP-1 INAIFFQGDWRRKFG--EPAESNFSISATENRLVPMLRETR-DYFYNKDD-------EWQ 213
hNS INAVYFKGNWKSQFRPENTRTFSFTKDDESEVQIPMMYQQGEFYYGEFSDGSNEAGGIYQ 240
mNS INAVYFKGNWKSQFRPENTRTFSFTKDDESEVQIPMMYQQGEFYYGEFSDGSNEAGGIYQ 240
VLSLPYKDTSFALSIFLPKTRFGLSEALQNLDSVTIQQLMSNTSNTLVNIAMPKWKIETA 280
SRP-7_ VLSLPYKDNTFALTIFLPKTRFGLTESLKTLDSATIQHLLSNVSSTSVNVQIPKWKIETK 271
SRP-2 VLSLKYADPKFTLAIFLPKQRFGLVDALEKINGEYIQNLLNDLKSSYVSVQIPKFKIEKE 266
SRP-3 VLHVAYSDQRYQFSVFLPKLRNSLKEALKKLNEKRFNDLLKTKKRTFMNTQLPKFTIEKD 268
SRP-1 VIGIPFKDKSAWFAIFLPTRRFALAENLKSLNAAKFHNLINNVYQEYIFLTFPKFKMDYK 273
hNS VLEIPYEGDEISMMLVLSRQEVPLATLEPLVKAQLVEEWANSVKKQKVEVYLPRFTVEQE 300
mNS VLEIPYEGDEISMMLALSRQEVPLATLEPLLKAQLIEEWANSVKKQKVEVYLPRFTVEQE 300
LGLNRALMAVGIEKAFTDSADLSNFADG--IYISQAAHKALIEVDEDGTVAAAATTISFS 338
SRP-7_ LGLEEALQSLGIKKAFDNDADLGNMADG--LYVSKVTHKALIEVDEEGTKAAAATTVSIS 329
SRP-2 LDLKETLEAIGIKEIFAEGADLSGIADK--VFISSGIHKAIIEVDEDGTTAAAAS--AFK 322
SRP-3 LNLKSHLQTLGITDIFSDSADLSGLAEN--LKISEGVHKAIIEVNEEGTTAAAVT--MMK 324
SRP-1 INLKTALAKFGLAELFTEQADLSGIGPG--LQLASATHQALIEVDQVGTRAAAAT--EAK 329
hNS IDLKDVLKALGITEIFIKDANLTGLSDNKEIFLSKAIHKSFLEVNEEGSEAAAVS----G 356
mNS IDLKDILKALGVTEIFIKDANLTAMSDKKELFLSKAVHKSCIEVNEEGSEAAAAS----G 356
LTSVFIPAEEPIEFTADHPFLFILS--KDNHPLFIGIHN--------------- 375
SRP-7_ LKSAMFVMEEPKDFTADHPFFFVLS--KDNHPLFVGLHH--------------- 366
SRP-2 VQLEMMIMAEPTQFVADHPFLFAVL--FENHTLFLGVHA--------------- 359
SRP-3 AVPMSARMEQPVNFIADHPFFFTIT--FLNHPIFVGVFNG--------------- 362
SRP-1 IFFTSASSDEPLHIRVDHPFLFAII--KDNSPLFLGTYT--------------- 366
hNS MIAISRMAVLYPQVIVDHPFFFLIRNRRTGTILFMGRVMHPETMNTSGHDFEEL 410
mNS MIAISRMAVLYPQVIVDHPFLYLIRNRKSGIILFMGRVMNPETMNTSGHDFEEL 410

Figure S1 Comparison of neuroserpin and SRP-1, 2, 3, 6, 7. Shown is the alignment of human (hNS) and mouse (mNS) neuroserpin with SRP-1, SRP-2, SRP-3, SRP-6 and SRP-7. Sites causing FENIB are shown in red and amino acids forming a hydrophobic pocket in green (* identical amino acids; : and . amino acids with similar characteristics). SRP-4 and SRP-5 were not further considered because they lack essential features of serpins.

Identities and similarities between SRP-1, 2, 3, 6, 7 and hNS or mNS are as follows:

hNS - SRP-1:
Identity: 103/422 (24.4%)
Similarity: 198/422 (46.9%)

hNS - SRP-2:
Identity: 129/416 (31.0%)
Similarity: 220/416 (52.9%)

hNS – SRP-3:
Identity: 125/419 (29.8%)
Similarity: 198/419 (47.3%)

hNS - SRP-6:
Identity: 114/432 (26.4%)
Similarity: 205/432 (47.5%)

hNS - SRP-7, isoform a:
Identity: 106/418 (25.4%)
Similarity: 208/418 (49.8%)

mNS - SRP-1:
Identity: 102/415 (24.6%)
Similarity: 196/415 (47.2%)

mNS - SRP-2:
Identity: 125/416 (30.0%)
Similarity: 218/416 (52.4%)

mNS - srp-3:
Identity: 120/427 (28.1%)
Similarity: 198/427 (46.4%)

mNS – SRP-6:
Identity: 111/426 (26.1%)
Similarity: 204/426 (47.9%)

mNS - SRP-7, isoform a:
Identity: 112/418 (26.8%)
Similarity: 210/418 (50.2%)

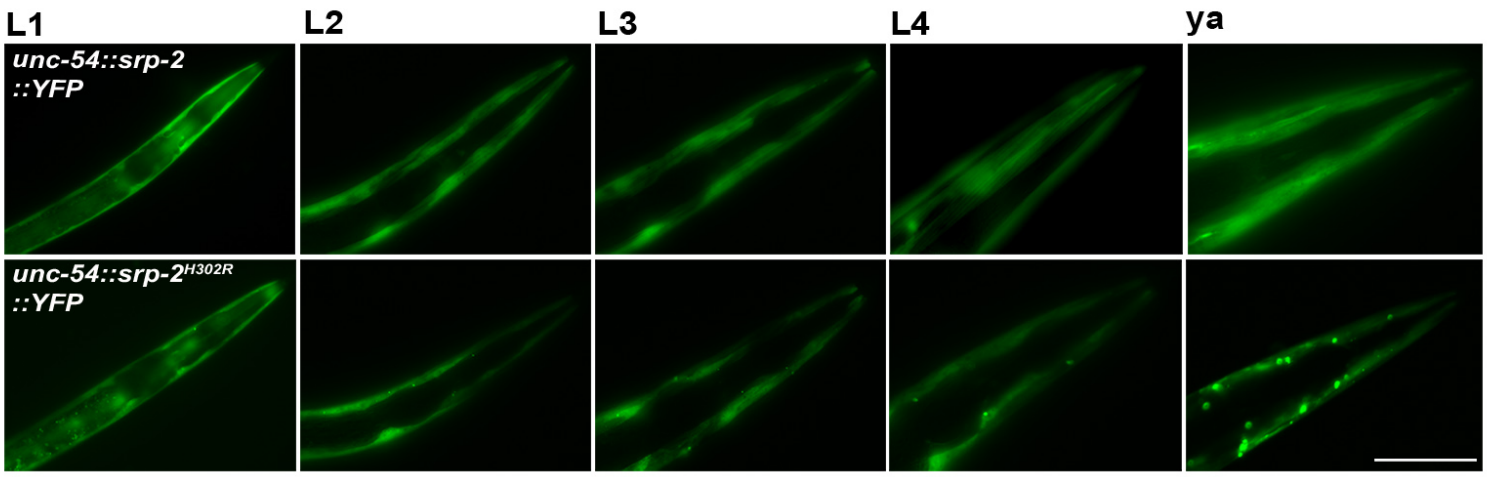

Figure S2 Kinetics of accumulation of SRP-2^{H302R} in muscle. Time course analysis (L1 (larval stage) to ya (young adult)) of SRP-2 (wild-type) and SRP-2^{H302R} expressed under a muscle-specific promoter in *C. elegans*. Only SRP-2^{H302R} forms protein aggregates from L4 onwards. Scale bar is 50µm.

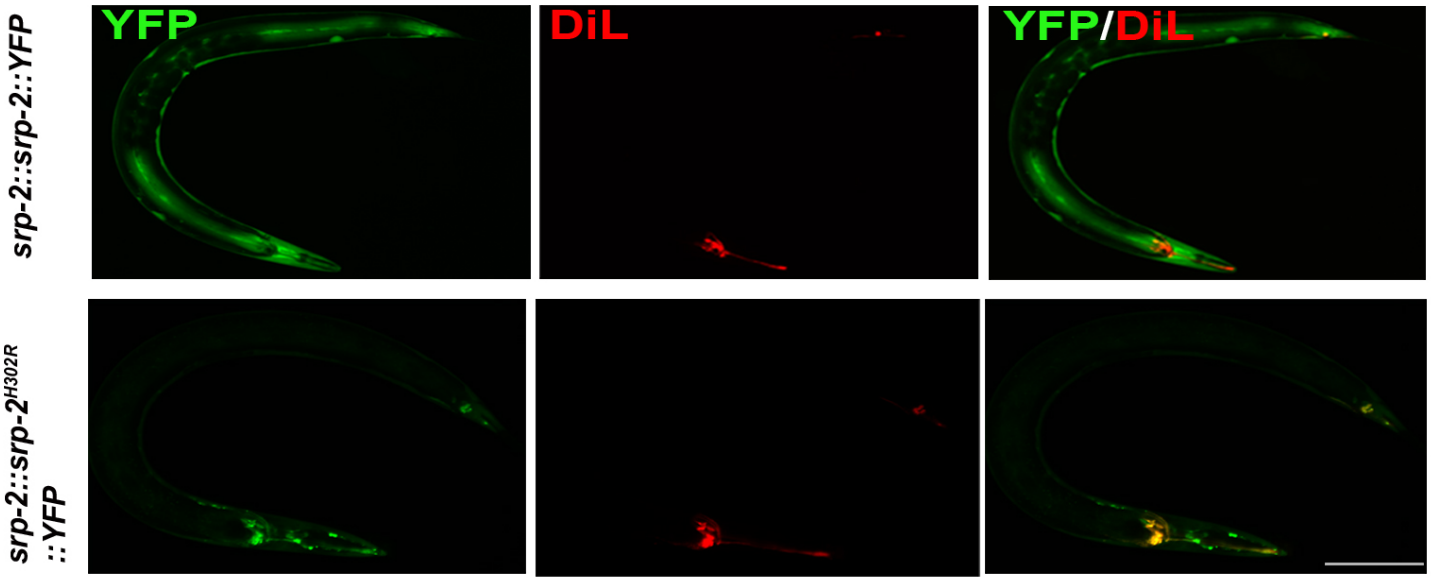

Figure S3 SRP-2 and SRP-2^{H302R} are expressed in phasmid neurons. Expression of SRP-2 and SRP-2^{H302R} (YFP) under their endogenous promoter co-stained with DiL (DiL) a marker of sensory neurons. SRP-2 and SRP-2^{H302R} co-localise with DiL in phasmid neurons of *C. elegans*. Scale bar is 50µm.

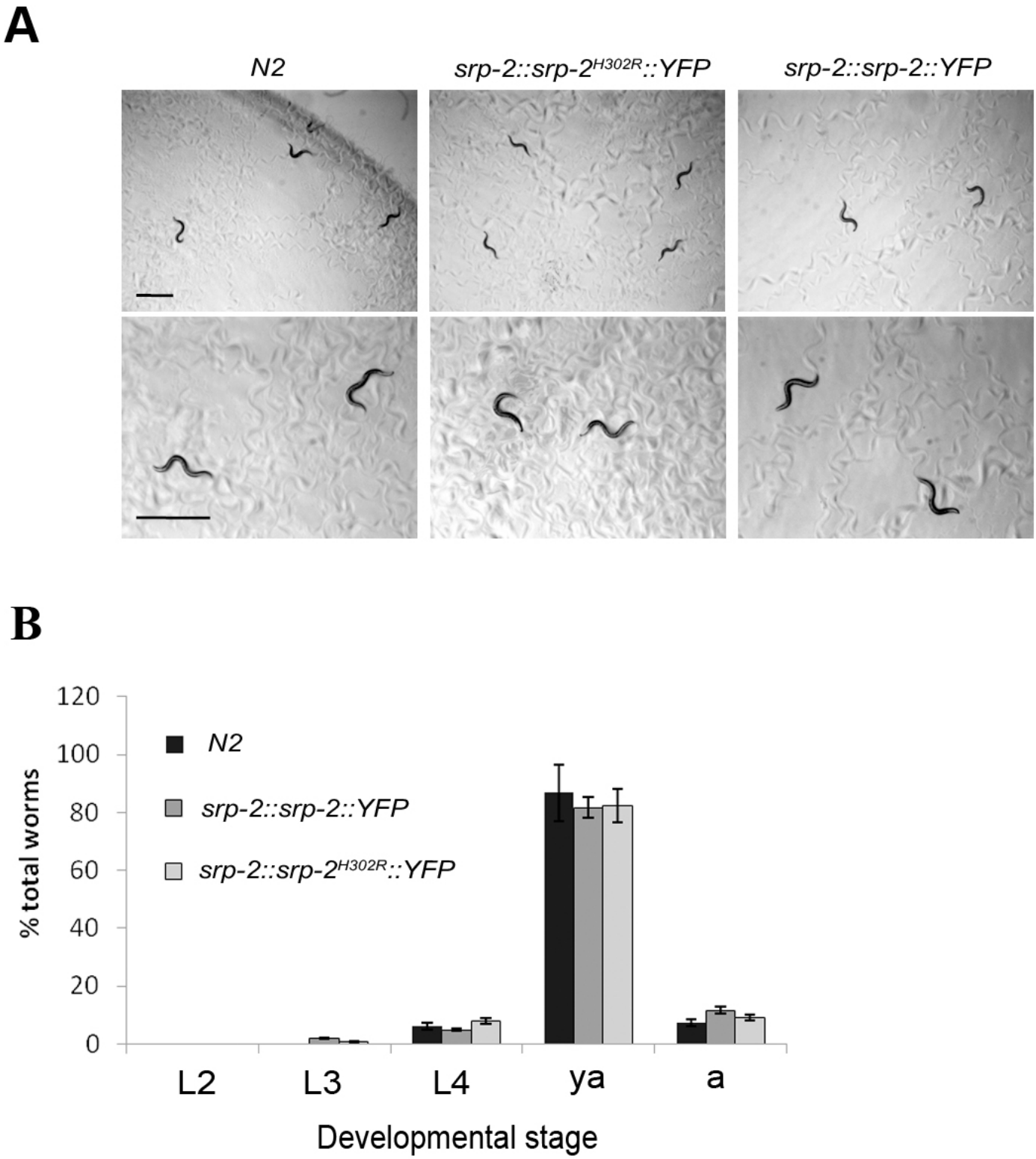

Figure S4 Mild SRP-2 or SRP-2^{H302R} overexpression has no influence on development. (A) Representative images of a synchronized population of N2, *srp-2::srp-2::YFP* or *srp-2::srp-2^{H302R}::YFP* embryos grown for 65h at 20°C. (B) Quantification of the developmental stage of worms described in (A) (n~200). No significant developmental differences were determined. Scale bars: 1 mm; statistical significance ns $p \geq 0.05$ (two tailed students *t*-test).

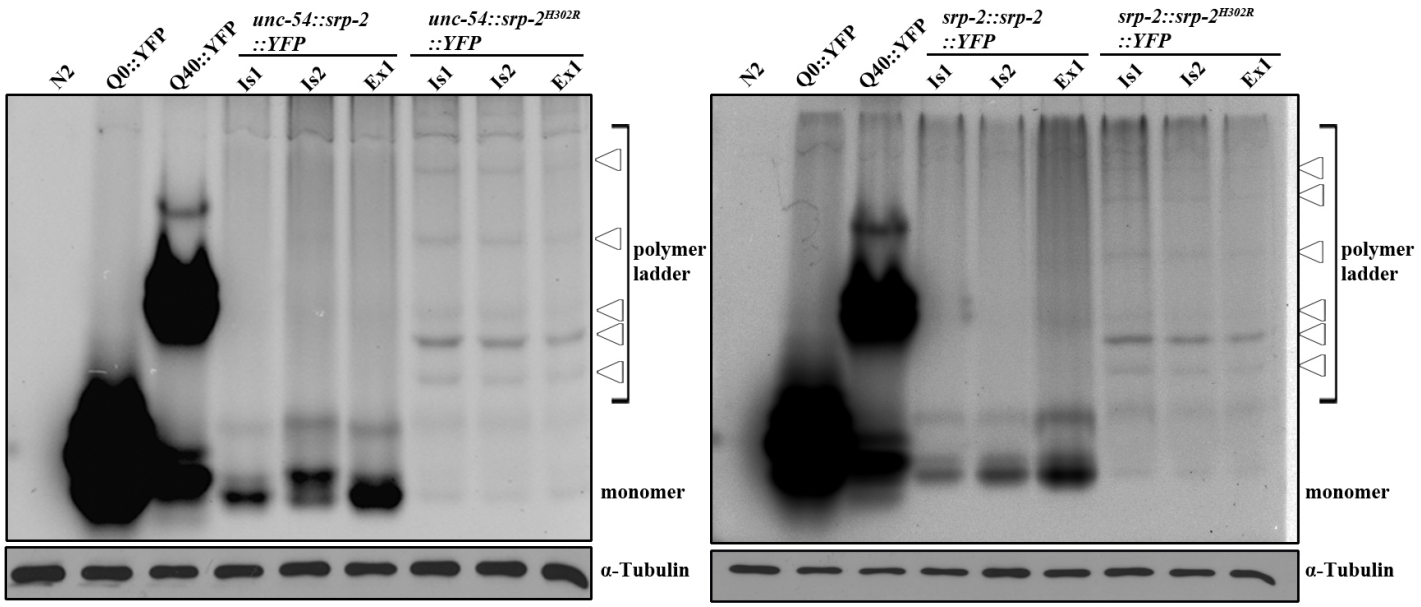

Figure S5 Comparison of expression of SRP-2^{wt} and SRP-2^{H302R} when expressed under the srp2 and unc54 promoter. Shown are 7.5 % native PAGE (visualized by scanning of GFP signal) of extracts from three SRP-2^{wt} (two with integrated transgene, Is1, Is2 and one with extrachromosmal transgene, Ex1) and three SRP-2^{H302R} (two with integrated transgene, Is1, Is2 and one with extrachromosmal transgene, Ex1) strains under control of the unc54 (left gel) and srp-2 (right gel) promoter. As controls, extracts from N2 wild-type (N2) and strains expressing 0 and 40 repeats of fluorescently tagged polyQ are shown (Q0, Q40). Expression levels of transgenically expressed GFP-labelled SRP-2 is higher when expressed under the unc54 promoter. Monomers can only been seen in lines expressing SRP-2^{wt}.

A

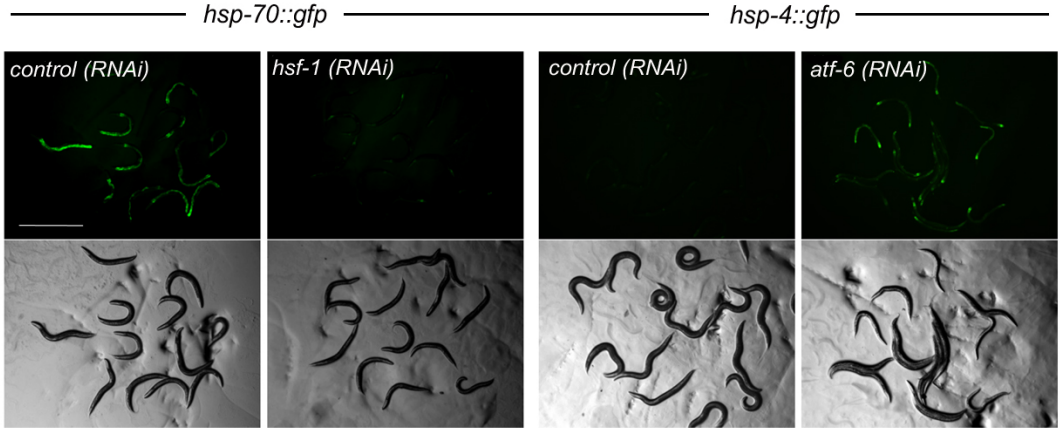
hsp-70::gfp
hsp-4::gfp
control (RNAi)
hsf-1 (RNAi)
control (RNAi)
atf-6 (RNAi)

B

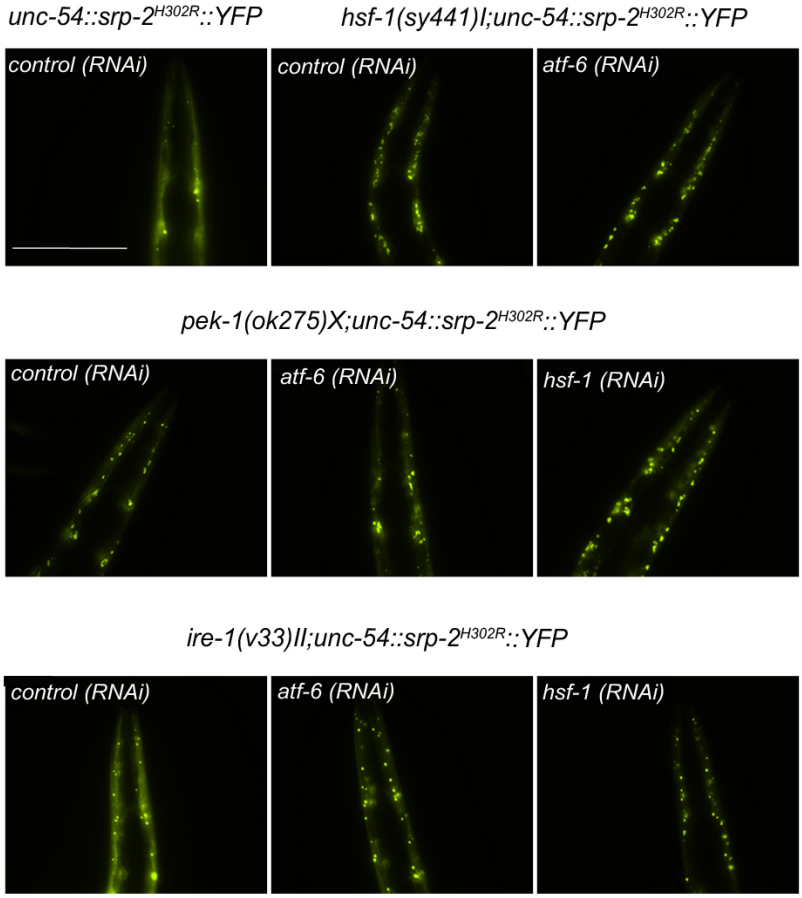
unc-54::srp-2H302R::YFP
hsf-1(sy441)I;unc-54::srp-2H302R::YFP
control (RNAi)
control (RNAi)
atf-6 (RNAi)
pek-1(ok275)X;unc-54::srp-2H302R::YFP
control (RNAi)
atf-6 (RNAi)
hsf-1 (RNAi)
ire-1(v33)II;unc-54::srp-2H302R::YFP
control (RNAi)
atf-6 (RNAi)
hsf-1 (RNAi)

C

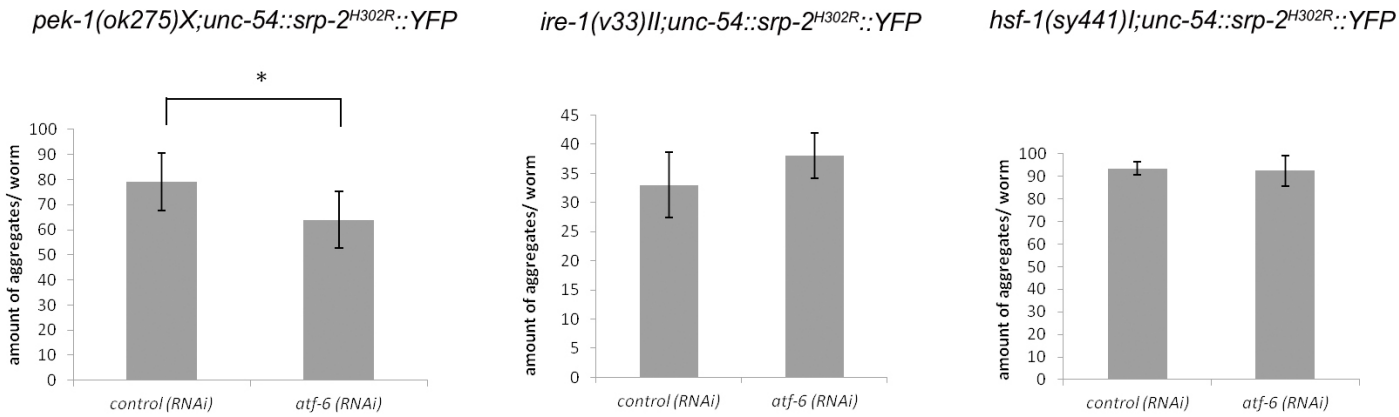
pek-1(ok275)X;unc-54::srp-2H302R::YFP
ire-1(v33)II;unc-54::srp-2H302R::YFP
hsf-1(sy441)I;unc-54::srp-2H302R::YFP
*
amount of aggregates/ worm
control (RNAi)
atf-6 (RNAi)

Figure S6 ***Hsf-1*** **but not** ***atf-6*** **depletion in UPR-deficient worms increase the amount of SRP-2^{H302R} aggregates in addition**. (A) Control for an efficient depletion of *hsf-1* or *atf-6* by RNAi. *Hsp-4::gfp* worms were feed for 48h with *aft-6* RNAi while *hsp-70::gfp* worms were treated for 48h with *hsf-1* RNAi and exposed to a 1h heat shock at 35°C following 4h recovery. The empty RNAi feeding vector pPD129.36 served as a control. *atf-6* depletion blocks a part of the UPR-pathway which results in an elevated stress response through *hsp-4* expression. A depletion of *hsf-1* prevents the activation of *hsp-70* after heat stress. (B) Representative fluorescence images of SRP-2^{H302R} worms lacking *hsf-1, ire-1* or *pek-1* after depletion of *hsf-1* or *atf-6* by RNAi. (C) Quantification of aggregates of SRP-2^{H302R} worms described in (B) after *atf-6* RNAi treatment (n=25). Scale bars: A 1 mm and B 100 µm; statistical significance * $p \leq 0.05$; ns $p \geq 0.05$ (two tailed students *t*-test).

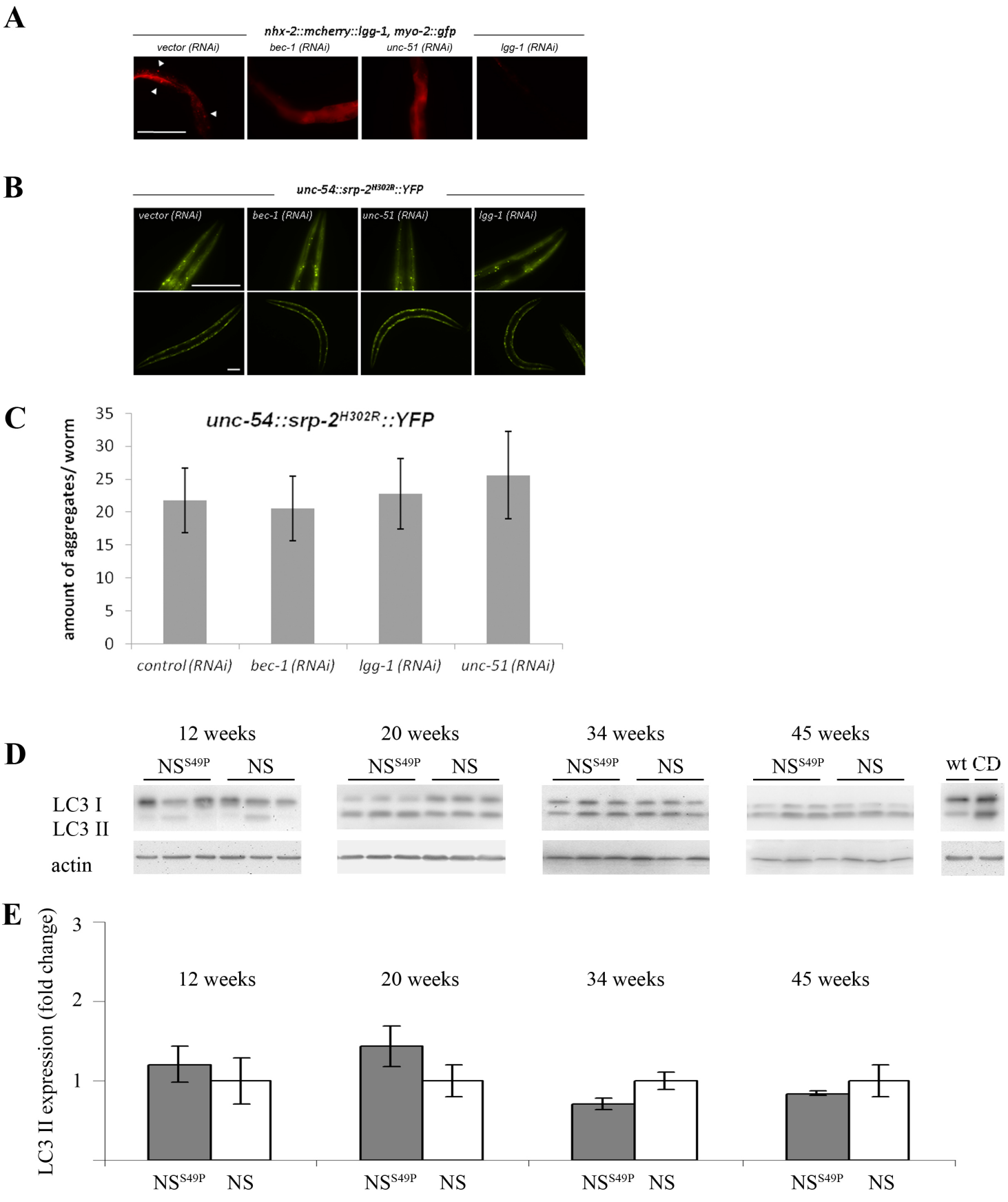

Figure S7 Autophagy does not contribute to clearance of SRP-2^{H302R} aggregates and is not induced in FENIB mice. (A) Control for efficient inhibition of autophagy. *mcherry::lgg-1* worms were treated with *bec-1, lgg-1, unc-51* or empty vector RNAi (control) for 48h following 4h starvation to induce autophagy. Animals treated with vector RNAi showed a punctuated distribution of *mcherry::lgg-1*, visualizing autophagosome formation, while treatment with *bec-1* or *unc-51* RNAi results in a diffuse distribution and feeding with *lgg-1* RNAi in a reduction of *mcherry::lgg-1* fluorescent, indicating autophagy inhibition. (B) Representative fluorescent images of SRP^{H302R} worms after depletion of indicated genes by RNAi. (C)

Quantification of aggregates of SRP-2^{H302R} worms described in (B) (n=15). No significant differences of SRP-2^{H302R} aggregates were visible. Scale bars: A and B 100 µm; statistical significance ns $p \geq 0.05$ (two tailed students *t*-test).(D) Activation of autophagy in FENIB mice was assessed by determining the levels of the autophagic marker protein microtubule-associated protein 1 light chain 3 -II (LC3-II) in *Tg*(NSwt) and *Tg*(NSS49P) mice aged 12, 20, 34 and 45 weeks by western blotting. (E) Densitometric quantification of LC3-II levels normalized to actin as a loading control revealed no significant differences between *Tg*(NSwt) and *Tg*(NSS49P) mice. Data are presented as mean ±SD, n = 3 per age. *Tg*(NSwt) values were set to 1. As positive control, brain extracts from a Cathepsin D knockout mouse (CD-/-) was used. Here autophagy is dramatically induced (as shown by the increased levels of LC3-II) when compared to mice with Cathepsin D (CD).

Table S1: Statistical analysis of SRP-2^{H302R} aggregate formation presented in Fig 4F.

Strain	RNAi	Exp. \ worm	1	2	3	4	5	6	7	8	9	10	11	12	13	14	15	mean aggregates/ worm	SEM	p-value (t-test)
pek-1(ok275)X; unc54::srp^{H302R}	*control*	1	83	75	84	53	63	105	84	98	76	65	83					79,00	± 11,45	
	hsf-1		129	96	138	90	139	108	95	158	101	76						113,00	± 22,4	1,60E-03
	control	2	89	84	71	86	55	67	72	83								75,88	± 9,63	
	hsf-1		112	128	114	106	100	114	125	93	93	83						106,80	± 11,8	1,65E-03
	control	3	44	34	64	52	40	50	10	28	39	23	33	46	56	41	44	40,27	± 9,98	
	hsf-1		58	47	58	65	48	75	58	85	106	48	79	83	99	69		69,86	± 15,41	4,08E-05
ire-1(33v)II; unc54::srp^{H302R}	*control*	1	37	31	33	24	34	42	26	34	23	46						33,00	± 5,6	
	hsf-1		56	43	54	48	41	30	48	39	43	33	52	38	30			42,69	± 6,95	1,03E-02
	control	2	33	32	38	30	42	28	36	29	35	29	34					33,27	± 3,39	
	hsf_1_2		36	47	47	48	42	57	50	51	46	46	55					47,73	± 4,07	1,75E-06
	control	3	25	33	28	28	30	29	27	21	25	30	40	33	33			27,46	± 3,42	
	hsf-1		30	45	34	43	32	35	24	36	33	44	28	38				32,67	± 5,03	1,77E-02